

Article

CLTSA: A Novel Tunicate Swarm Algorithm Based on Chaotic-Lévy Flight Strategy for Solving Optimization Problems

Yi Cui, Ronghua Shi and Jian Dong * 

School of Computer Science and Engineering, Central South University, Changsha 410083, China

* Correspondence: dongjian@csu.edu.cn

Abstract: In this paper, we proposed a tunicate swarm algorithm based on Tent-Lévy flight (TLTSA) to avoid converging prematurely or failing to escape from a local optimal solution. First, we combined nine chaotic maps with the Lévy flight strategy to obtain nine different TSAs based on a Chaotic-Lévy flight strategy (CLTSA). Experimental results demonstrated that a TSA based on Tent-Lévy flight (TLTSA) performed the best among nine CLTSAs. Afterwards, the TLTSA was selected for comparative research with other well-known meta-heuristic algorithms. The 16 unimodal benchmark functions, 14 multimodal benchmark functions, 6 fixed-dimension functions, and 3 constrained practical problems in engineering were selected to verify the performance of TLTSA. The results of the test functions suggested that the TLTSA was better than the TSA and other algorithms in searching for global optimal solutions because of its excellent exploration and exploitation capabilities. Finally, the engineering experiments also demonstrated that a TLTSA solved constrained practical engineering problems more effectively.

Keywords: tunicate swarm algorithm; chaotic mapping; Lévy flight strategy; benchmark test functions; engineering design problems; meta-heuristic

MSC: 68W50**Citation:** Cui, Y.; Shi, R.; Dong, J.CLTSA: A Novel Tunicate Swarm Algorithm Based on Chaotic-Lévy Flight Strategy for Solving Optimization Problems. *Mathematics* **2022**, *10*, 3405. <https://doi.org/10.3390/math10183405>

Academic Editor: José Antonio Sanz

Received: 2 August 2022

Accepted: 15 September 2022

Published: 19 September 2022

Publisher's Note: MDPI stays neutral with regard to jurisdictional claims in published maps and institutional affiliations.



Copyright: © 2022 by the authors. Licensee MDPI, Basel, Switzerland. This article is an open access article distributed under the terms and conditions of the Creative Commons Attribution (CC BY) license (<https://creativecommons.org/licenses/by/4.0/>).

1. Introduction

Because of the rapid pace of scientific development and innovation, more and more engineering design problems need urgent optimization. The problem is to avoid local solutions yet maintain the optimization trend, and that is the focus of this research [1]. Many of these issues involve complicated nonlinear constraints and high dimensions [2,3]. However, traditional gradient-based optimization methods rely excessively on a large amount of gradient information. When the target engineering problem has more constraints or more extreme values, the gradient search becomes inefficient, that is, the optimal solution obtained may not be the global optimal solution. Therefore, traditional optimization methods are no longer suitable for solving complex engineering design problems.

In recent years, researchers have applied meta-heuristic algorithms because of their high efficiency, wide applicability, and expandability. Most have been proposed after watching and studying natural phenomena or the behavior of creatures. According to different inspiration sources, these algorithms can be divided into four categories: swarm intelligence (SI) algorithms, evolutionary algorithms (EAs), physics-based algorithms, and human-based algorithms. The evolutionary algorithms, inspired by the theory of evolution by natural selection, simulate the crossover, mutation, selection, and other evolutionary behaviors in the process of biological evolution, such as genetic algorithms (GAs) proposed by Holland [4]. Physics-based algorithms are inspired by physical phenomena in nature, such as simulated annealing (SA) algorithm [5], black hole (BH) algorithm [6], central force optimization (CFO) [7], water cycle algorithm (WCA) [8], and lightning attachment procedure optimization (LAPO) [9]. Human-based algorithms are mainly inspired by

human behaviors, such as human teaching behaviors, social behaviors, learning behaviors, emotional behaviors, and management behaviors. For example, teaching-learning-based-optimization (TLBO) simulates teaching and learning behaviors [10]. Political optimizer (PO) builds a model based on the multistage process of politics [11,12].

The particle swarm algorithm (PSO) proposed by Kennedy and Eberhart is one of the most widespread and successful [13,14]. By studying the cooperative predation behavior of birds, PSO uses information sharing among individuals in the population to find the global optimal solution, which may enable the algorithm to jump from the local optimal solution. As PSO is paid more attention, more and more swarm intelligence algorithms like PSO are proposed, such as ant colony optimization (ACO) [15], artificial bee colony (ABC) algorithm [16], glowworm swarm optimization (GSO) [17], cow search algorithm (CSA) [18], sailfish optimizer (SFO) [19], Harris hawks optimization (HHO) [20,21], manta ray foraging optimization (MRFO) [22], and mayfly algorithm (MA) [23]. In general, swarm intelligence algorithms are superior to evolutionary algorithms in some respects, for example, each individual can improve their fitness by updating position, which enhances the search efficiency of the population. While in evolutionary algorithms, only the current best individuals and descendants produced similar to them in terms of features are allowed to enter the subsequent iterations, individuals with poor fitness are discarded. In addition, swarm intelligence algorithms are easier to use because of fewer operators [24,25].

Although different algorithms have their advantages, their whole optimization processes can be regarded as the combination of the exploration phase and exploitation phase. In the exploration phase, the algorithm produces a population as random as possible to explore a potential promising area in the search space. In the exploitation phase, it attempts to develop the promising region found in the previous phase to search for the optimal solution.

Chaos, randomness generated by a deterministic system, is an important concept in nonlinear dynamics [26,27]. Chaotic mapping, because of its traversal behavior and randomness, has wide application in the search to optimize meta-heuristic algorithms [28]. At present, improved meta-heuristic algorithms based on chaotic maps include chaotic artificial bee colony (CABC) algorithm [29], chaotic grey wolf optimization (CGWO) algorithm [30], chaotic butterfly optimization algorithm (CBOA) [31], chaotic firefly algorithm (CFA) [32], and so on.

Although algorithms based on chaotic mapping can escape the local optimal solution, they have weak exploration. To enhance it while maintaining a balance with exploitation, the introduction of the Lévy flight strategy is an effective method. Lévy flight is a random walk strategy with step size that satisfies the Lévy distribution; the research has found that many animals' behavior obeys it [33]. For example, animals move around an existing food source, but they occasionally travel long distances in search of a new food source [34,35]. The small sizes of Lévy flight allow the algorithm to exploit regions near the current solution. In addition, a long-distance movement sporadically generated by Lévy flight enables the algorithm to jump out of the local optimal solution. When combined with chaotic mapping, it produces a step size with greater randomness. From this perspective, it is feasible to apply the chaotic mapping mechanism to Lévy flight.

In this study, an improved tunicate swarm optimization algorithm based on a Chaotic-Lévy flight strategy (CLTSA) is proposed to solve the shortcomings of the original TSA. The strategy is introduced when the search agents move toward the current solution so that they can update their positions according to the randomly generated step sizes. The next sections of this paper are displayed as follows: In Section 2, the inspiration, principle, and mathematical model of the TSA are introduced. Next, several common chaotic maps, Lévy flight strategy, and application of the two optimization methods to improve the TSA are described. In the fourth and fifth sections, the TL TSA, as the best performer among CLTSAs, is selected to evaluate the capability of optimizing benchmark functions by comparing them with other well-known meta-heuristic algorithms to measure the capability of TL TSA to solve practical engineering problems. The article concludes in Section 6.

2. Related Work

Various works recently investigated the use of Lévy flight in swarm intelligence algorithms. Lévy flight refers to a random walk in which the probability distribution of the step size is heavy tailed. There is a relatively high probability of large strides in the random walk, which is widely used to improve swarm intelligence optimization algorithms. Yang et al. proposed a cuckoo search algorithm (CS) [36] based on Lévy flight, in which search logic simulates the breeding behavior of cuckoos. The algorithm first generates n initial positions called nests. Then, a new nest is generated using the Lévy flight mechanism and compared to the solution of the random nest: If the fitness value of the new position is better than the previous one, the new solution is used to replace the previous one. In each iteration, some of the worst solutions are replaced to obtain a better set of nest positions, such that the process is executed until the optimal solution is found. Another optimization algorithm based on Lévy flight is the Lévy flight whale optimization algorithm (LWOA) [37]. The whale's predation strategy mainly includes three behaviors: encircling prey, bubble-net attacking, and find prey. Most of the development of search agents take place in bubble-net attacking. Due to the trajectories of humpback whales during prey being spiral, the search agent moving towards the food will be replaced by a new random position on spiral curve. In LWOA, the performance of the algorithm is improved by replacing the spiral walk with the Lévy flight strategy. The Lévy flight strategy is also introduced in flower pollination algorithm (FPA) [38]. According to the FPA, each pollen particle represents a solution that walks in the search space under two different search rules: local pollination and global pollination. For each step, one of the update rules is selected stochastically: If the local pollination is selected, the pollen particle walks in a limited around area, and the step-size is multiplied by a random number generated by the uniform distribution $U(0,1)$; if the selected movement is global pollination, the pollen particle walks toward the global optimal solution, and the step-size is multiplied by a random number generated by the Lévy flight. Amirsadri et al. introduced LF-based grey wolf optimization algorithm blended with back propagation (LF-BP-GWO) [39] to train neural networks. First of all, the Lévy flight is applied to improve the exploration ability of GWO. Then, the back propagation which enhances the exploitation ability in combination with improved GWO was used to train neural network. Each individual in the proposed LF-BP-GWO is considered as the weights and the biases set in the neural network. As a random walk strategy, Lévy flight generates a large step size that keeps a small number of search agents away from the current optimal solution, which enhances the algorithm's exploration ability; the generated small step size allows most search agents to continue at the current optimal solution development near the solution, thus balancing the exploration and development of the algorithm.

Chaotic mapping is used to generate chaotic sequences, which are sequences of randomness produced by simple deterministic systems. In the field of optimization, chaotic mapping can be used as an alternative to pseudo-random number generators, generating chaotic numbers between 0 and 1, often with better results than pseudo-random numbers. Chaotic mapping is also widely used in swarm intelligence algorithms. Bilal Alatas proposed three chaotic artificial bee colony algorithms (CABC) [29]: CABC1, CABC2, and CABC3. According to CABC1, the use of the chaos mapping is mainly reflected in the population initialization period. Through chaotic mapping, a set of initial populations with better diversity are generated. In CABC2, if a solution called food is not enhanced by a defined number of trials, the hired bee will give up the position and the scout bee of this hired bee will perform chaotic search for a better food source. CABC3 is a combination of the above two improved algorithms. It not only uses the selected chaotic map to generate a diverse initial population, but also performs chaotic search. Mohammad Tubishat et al. proposed an improved Sine cosine algorithm (ISCA) for Hadith classification [40]. The first modification includes replacing a random number with a chaotic sequence generated by a singer map. This modification allows ISCA to control the switching between sine and cosine equations, which are applied to update the position of search agents. The second modification is improving development ability by combining with simulated annealing.

At the end of each iteration, the best solution obtained by SCA will be considered as the initial solution of simulated annealing. If simulated annealing finds a better solution, it will replace the current optimal solution with new one. Talatahari et al. improved the traditional algorithm and proposed a chaotic imperialist competitive algorithm (CICA) [41]. Through the comparative research and evaluation of different chaos maps, the experimental results proved the superiority of logistic and sinusoidal maps. In order to enhance the global exploration ability, the firefly algorithm (FA) [32] also introduces chaotic mapping to set light and other absorption parameters. The results show that the Gaussian map has the best effect as the absorption coefficient. The chaotic mapping is also applied to improve KH algorithm [42]. According to CKH, many types of movements of krill are proposed using different chaotic maps, among which the singer map performs best.

The TSA has received a lot of attention because of its simplicity and optimal. E. H. Houssein et al. introduced the local escape operator into TSA (TSA-LEO) to enhance its optimization effect [43]. In the TSA-LEO, several solutions such as the best position, two randomly generated individual, two randomly selected individual, and a new randomly generated individual were used to obtain the alternative solutions with excellent performance of the algorithm. Specifically, the TSA-LEO enhances the quality of solutions by updating their positions under some criteria. The TSA-LEO was further tested on a real-world problem, namely, segmentation based on the objective functions of Otsu and Kapur, and solved multilevel threshold problems while seeking the optimal thresholds for image separation. F. S. Gharehchopogh proposed an improved TSA with best-random mutation strategy (QLGCTSA) [44]. According to the QLGCTSA, the Quantum Rotation Gate mechanism, Lévy Mutation, Cauchy Mutation, and Gaussian Mutation were used to enhance the TSAs' performance. These methods have different functions, increasing the QLGCTSA's performance at a given stage in the optimization operation. The quantum rotation gate was proposed to increase the population diversity; Lévy flight enabled each individual to find better position and increase the ability to search deeper; Cauchy mutation was used to modify the capability to search in search agents or add neighbors of each generation; and Gaussian mutation helped the algorithm execute the global exploration. Table 1 is the comparison of improved algorithms.

Table 1. Comparison of algorithms involved in related work.

| Year | Algorithm | Method Used | Application Area(s) | Shortcoming |
|------|----------------|--|---|--|
| 2013 | CS [36] | Lévy flight | Global optimization | |
| 2018 | LWOA [37] | Lévy flight | Global optimization | poor global exploration ability |
| 2012 | FPA [38] | Lévy flight | Nonlinear design benchmark and global optimization | |
| 2017 | LF-BP-GWO [39] | Lévy flight Back propagation | Neural network | poor global exploration ability and running slow |
| 2010 | CABC [29] | Chaotic mapping | Global numerical optimization | |
| 2022 | ISCA [40] | Singer chaotic map simulated annealing | Feature selection problem for Hadith classification | |
| 2012 | CICA [41] | Chaotic mapping | Truss structures design problem | poor solution accuracy |
| 2014 | CKH [42] | Chaotic mapping | Global optimization | |
| 2021 | TSA-LEO [43] | Local escape operator | Global optimization and Image segmentation | |
| 2022 | QLGCTSA [44] | Quantum Rotation Gate Lévy flight Cauchy Mutation Gaussian Mutation | Numerical optimization CEC2017 and engineering design problem | unbalanced exploration and development and high computational complexity |

3. The Proposed CLTSA

3.1. TSA

The TSA was proposed by Kaur et al. after observing the social behavior of a tunicate searching for prey [45]. In the process of hunting, this marine invertebrate uses water jets and swarm intelligence to search for prey. Each tunicate can quickly discharge previously inhaled seawater through the siphons of the atrium, generating a kind of jet propulsion, which propels it rapidly. Moreover, tunicates display swarm intelligence when they share search information about the location of food. To establish the mathematical model of its jet propulsion mechanism, the tunicate is required to meet the following three important constraints:

- Avoiding clashes between each search agent.
- Each agent is guaranteed to move in the direction of the optimal individual.
- Make the search agents converge to the region near the optimal individual.

3.1.1. Avoiding Clashes between Each Search Agent

To prevent search agents from generating unnecessary clashes, the following formulas are used to calculate the new location of the agent:

$$\vec{A} = \frac{\vec{G}}{M} \tag{1}$$

$$\vec{G} = c_2 + c_3 - \vec{F} \tag{2}$$

$$\vec{F} = 2 \cdot c_1 \tag{3}$$

where \vec{A} is a vector used to find the new position of each agent; \vec{G} is gravity; \vec{F} is the water flow in the deep sea; and $c_1, c_2,$ and c_3 are three random numbers in the interval 0 to 1 inclusive. \vec{M} is a vector the value of which is expressed as the social strength between the search agents and is defined as:

$$\vec{M} = P_{min} + c_1 \cdot (P_{max} - P_{min}) \tag{4}$$

where P_{min} and P_{max} indicate the incipient and secondary speeds that enable search agents to build social interaction. In this paper, P_{min} and P_{max} are set to 1 and 4 respectively.

3.1.2. Move in the Direction of the Optimal Individual

After resolving clashes between adjacent search agents, each one should move toward the neighboring individual having the highest fitness value. The mathematical model of moving towards the best search agent is established as:

$$\vec{PD} = \left| X_{best} - r_{rand} \cdot X(t) \right| \tag{5}$$

where \vec{PD} is a vector that represents the spatial distance between the target food and the tunicate; X_{best} stands for food that is at the position of the current optimal individual; r_{rand} is a random number in the interval [0, 1]; and $X(t)$ stores the location information of the current search agent in the t -th iteration.

3.1.3. Make the Search Agents Converge to the Optimal Individual

To make the search agents carry out sufficient local exploration near the optimal individual to find the optimal solution of the current iteration, their locations are calculated by Equation (6):

$$X(t) = \begin{cases} X_{best} - \vec{A} \cdot \vec{PD}, & \text{if } r_{rand} < 0.5 \\ X_{best} + \vec{A} \cdot \vec{PD}, & \text{if } r_{rand} \geq 0.5 \end{cases} \quad (6)$$

At iteration t , each search agent explores the region near the optimal individual X_{best} and assigns the result to $X(t)$ to update its position.

3.1.4. Swarm Behavior

The swarm behavior of the tunicate transmits location information between the search agents. This mechanism is driven by the position of the current search agent in the next iteration and is obtained according to the position updated by the current search agent. This is done through the optimal individual and the position updated by the previous individual through swarm behavior. The mathematical model is defined as:

$$X_i(t+1) = \begin{cases} \frac{\vec{X}_i(t) + \vec{X}_{i-1}(t+1)}{2 + c_1} & \text{if } i > 1 \\ \vec{X}_i(t) & \text{if } i = 1 \end{cases} \quad (7)$$

where $i = 1, \dots, N$, N is the size of the tunicate population, $X_i(t+1)$ is the position of the current search agent in the next iteration, $X_{i-1}(t+1)$ is the position of the previous search agent in the next iteration, and $X_i(t)$ is computed by Equation (6).

To illustrate the detailed process of the TSA, the main steps to update the positions of search agents are listed below:

- Step 1: Initialize the original population of search agents \vec{X} .
- Step 2: Assign values to the max-iterations and other initial parameters.
- Step 3: Compute the fitness value of each tunicate and select the individual with the best fitness value as the optimal search agent.
- Step 4: Update the location of each search agent by Equation (7).
- Step 5: Keep each search agent in the search space.
- Step 6: Calculate the fitness value of each updated search agent; if there is a better individual than the previous optimal search agent in the population, update \vec{X}_{best} .
- Step 7: If the maximum iteration is reached, then the procedures stop. Otherwise, continue with steps 4–7.
- Step 8: Print the best individual (X_{best}) so far.

3.2. Lévy Flight

Lévy flight is a random walk strategy whose step size satisfies the Lévy distribution [46]. Having stable distribution with infinite mean value and divergent variance, it enables the search agents to generate a long jump distance during exploration. Another important advantage of the Lévy flight strategy is its combination of global exploration and exploitation. When search agents walk randomly, there are usually more small step sizes and a handful of large step sizes; therefore, the Lévy flight strategy not only helps the search agents to carry out a local search by jumping in small step sizes near the optimal solution but also enable the search agents to fully explore the unknown area of the search space by jumping in large step sizes. Above all, the small step sizes random walk ensures that the search agents carefully explore the area around the best individual and improve the possibility of the population's position in the search space. In addition, exploration

capability and mutation reflect the advantage in the global exploration. The Lévy flight strategy is mathematically defined as [47]:

$$L(s, \gamma, \mu) = \begin{cases} \sqrt{\frac{\gamma}{2\pi}} \cdot \exp\left[-\frac{\gamma}{2(s-\mu)}\right] \frac{1}{(s-\mu)^{\frac{3}{2}}}, & 0 < \mu < s < \infty \\ 0, & \text{otherwise} \end{cases} \tag{8}$$

where s is the samples; γ is a transmission parameter; and μ is the minimum step size. When $s \rightarrow \infty$, the above formula can be simplified as:

$$L(s, \gamma, \mu) \approx \sqrt{\frac{\gamma}{2\pi}} \cdot \frac{1}{s^{\frac{3}{2}}} \tag{9}$$

The Equation (9) is transformed into a Fourier transform:

$$F(k) = \exp\left[-\alpha|k|^\beta\right], 0 < \beta \leq 2 \tag{10}$$

where α is a transmission parameter. In general, the analytical form of Equation (10) is described as follows:

$$L(s) = \frac{1}{\pi} \int_0^\infty \exp\left[-\alpha|q|^\beta\right] \cos(qs) dq \tag{11}$$

$$L(s) \rightarrow \frac{\alpha\beta\Gamma(\beta) \sin\left(\frac{\pi\beta}{2}\right)}{\pi|s|^{1+\beta}}, s \rightarrow \infty \tag{12}$$

where $\Gamma(\beta)$ is the Gamma Function. In most cases, the most direct and effective method of symmetric, stable Lévy distribution is to use the Mantegna algorithm, which generates a random step size that satisfies the Lévy distribution. The random step size is calculated as follows [48,49]:

$$S = \frac{u}{|v|^{\frac{1}{\beta}}} \tag{13}$$

where u and v satisfy the following normal distribution [47]:

$$u \sim (0, \sigma_u^2), \quad v \sim (0, \sigma_v^2) \tag{14}$$

$$\sigma_u = \left[\frac{\Gamma(1 + \beta) \cdot \sin\left(\frac{\pi\beta}{2}\right)}{\Gamma\left[\frac{1+\beta}{2}\right] \beta \cdot 2^{\beta-\frac{1}{2}}}\right]^{\frac{1}{\beta}} \tag{15}$$

$$\sigma_v = 1 \tag{16}$$

where $0 < \beta < 2$ is a parameter that controls the shape of the distribution. In general, β directly affects the balance between development capability and exploration capability.

Figure 1 displays the Lévy flight trajectory of continuous moving 500 times with different β in a two-dimensional space. The study found that the range of step sizes is registered with maximal values in the range of $10^2 \times [-14, 2]$ for the x and $10^2 \times [-2, 12]$ for the y dimension when $\beta = 1$; the smallest in the range of $10^{-15} \times [-2, 10]$ for the x and $10^{-15} \times [-6, 2]$ for y dimension when $\beta = 2$; and kept a balance when $\beta = 1.5$ with range $[-100, 0]$ for the x and $[-10, 80]$ for the y dimension. Hence, β was set to 1.5 in this research. The factor S depended on the dimension of the problem to be solved; otherwise, the Lévy flight strategy showed high aggressiveness and generated solutions beyond the scope of the problem. It is obvious that the Lévy Flight strategy generates both small-step random walks and large-step random jumps in the search space, simultaneously taking into account development and exploration.

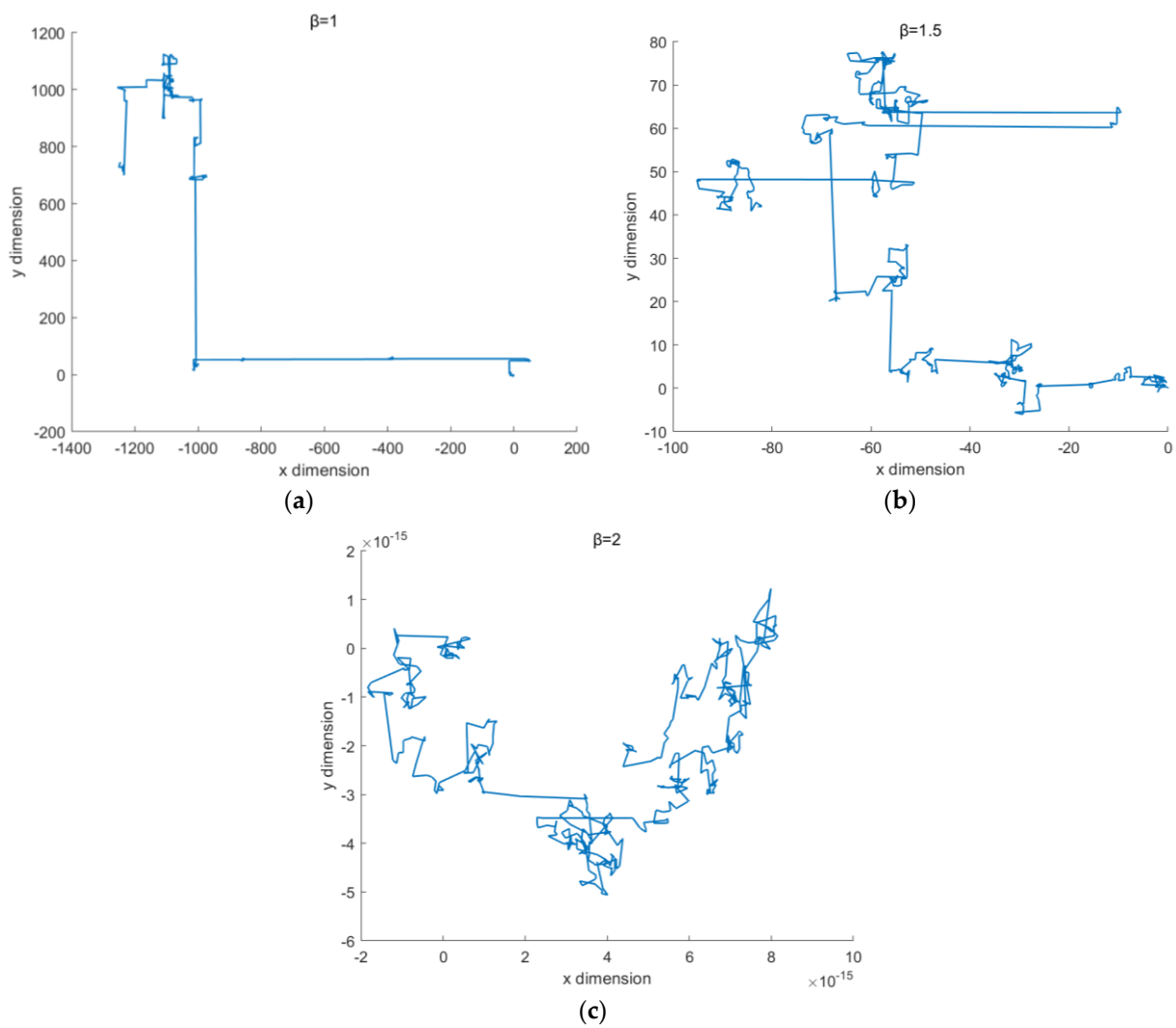


Figure 1. Lévy flight track in a two-dimensional search space with different β . (a) $\beta = 1$; (b) $\beta = 1.5$; (c) $\beta = 2$.

3.3. Chaotic Maps

Chaotic mapping is a mechanism used to generate random chaotic sequences generated by a simple deterministic system. These sequences have the characteristics of nonlinearity, ergodicity, non-repeatability, and randomness [50]. Therefore, chaotic sequences help search agents explore a search space more fully, make the algorithm escape from the local optimal solution, and increase the diversity of the population. In the field of optimization algorithms, chaotic maps are often more advantageous than pseudo-random number generators for generate chaotic numbers between 0 and 1 [51]. The common mapping functions are listed below, and their distribution graphs are shown in Figure 2:

- Chebyshev map

The mapping function of the Chebyshev map is defined as follows [52]:

$$x_{k+1} = \cos\left(\alpha \cos^{-1} x_k\right) \tag{17}$$

where α is a control parameter of the Chebyshev map.

- Circle map

The Circle map could be denoted by Equation (18) [53]:

$$x_{k+1} = x_k + \beta - \left(\frac{\alpha}{2\pi} \sin(2\pi x_k)\right) \text{mod}(1) \tag{18}$$

when α is set to 0.5 and β is set to 0.2, the circle map could generate stochastic numbers between 0 and 1.

- Gauss map

The Gauss chaotic numbers are calculated by the following equation [54]:

$$x_{k+1} = \begin{cases} 0, & \text{if } x_k = 0 \\ \frac{1}{x_k} \text{mod}(1) & \text{if } x_k \neq 0 \end{cases} \tag{19}$$

- Iterative chaotic map with infinite collapses (ICMIC)

The mapping function of the iterative map is listed below [55]:

$$x_{k+1} = \text{abs}\left(\sin\left(\frac{\alpha}{x_k}\right)\right) \tag{20}$$

where α is a parameter for controlling the chaotic map, and the iterative map could gain superior performance when $\alpha = 0.7$.

- Logistic map

The Logistic map is a one-dimensional nonlinear chaotic map and one of the most commonly used chaotic maps, and it is represented as follows [56]:

$$x_{k+1} = \alpha x_k(1 - x_k) \tag{21}$$

where α is a control parameter whose value is between 3.5 and 4 to make the Logistic map produce chaotic sequences. Generally, α is set to 4.

- Sine map

The Sine map is a unimodal map, it is given in Equation (22) [32]:

$$x_{k+1} = \frac{\alpha}{4} \sin(\pi x_k) \tag{22}$$

where α is a control parameter with a value range in (0, 4].

- Singer map

The mapping function of the Singer map is defined as follows [57]:

$$x_{k+1} = \alpha \left(7.86x_k - 23.31x_k^2 + 28.75x_k^3 - 13.203875x_k^4\right) \tag{23}$$

when the value of control parameter α is in (0.9,1.08), the Singer map could produce chaotic sequences.

- Sinusoidal map

The chaotic numbers of the Sinusoidal map are computed as [56]:

$$x_{k+1} = \alpha x_k^2 \sin(\pi x_k) \tag{24}$$

where α is set to 2.3 to generate chaotic numbers.

- Tent map

The Tent map is shown by Equation (25) [58]:

$$x_{k+1} = \begin{cases} \frac{x_k}{\alpha} & x_k \leq \alpha \\ \frac{(1-x_k)}{1-\alpha} & \alpha < x_k \leq 1 \end{cases} \quad (25)$$

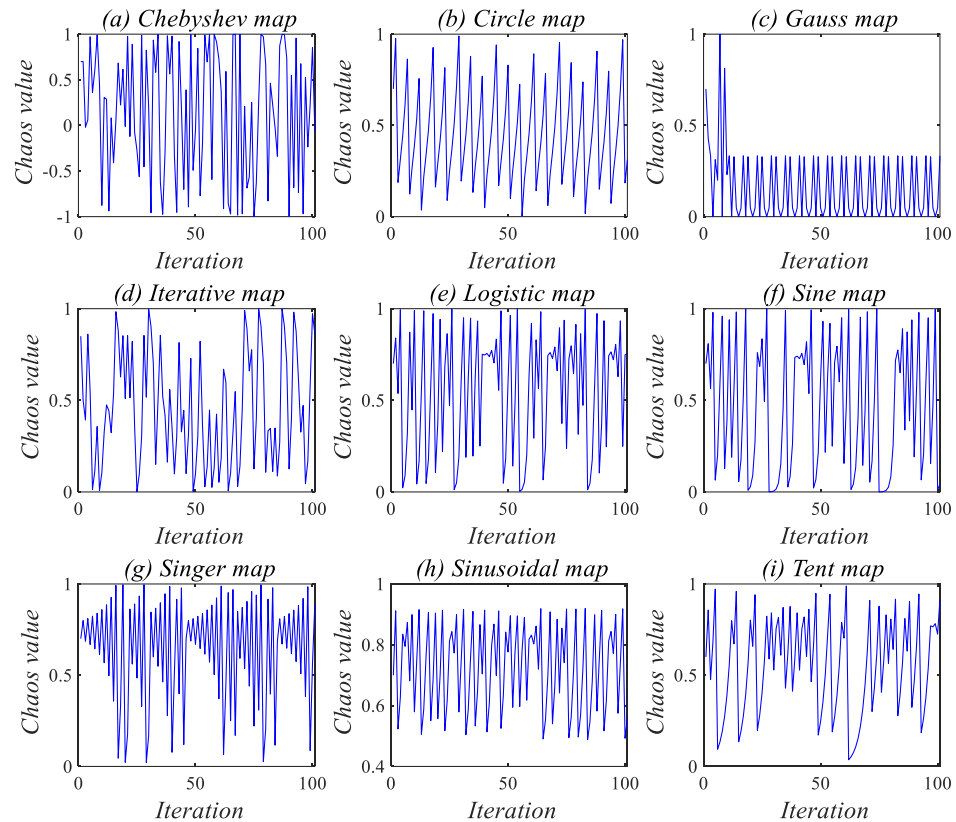


Figure 2. Distribution graphs of nine common chaotic maps.

3.4. Chaotic-Lévy Flight TSA

The current research shows that it is feasible to optimize the meta-heuristic algorithm by combining chaotic mapping and Lévy flight [59,60]. To solve the shortcomings of the TSA, such as falling easily into local optimal solutions and insufficient exploration [43], this section introduces an improved TSA from using the Chaotic-Lévy flight strategy (CLTSA). It allows search agents to find a suitable location in the area near the optimal solution, fully explore the search space, and avoid the emergence of a local optimal solution.

In this paper, the modification to the TSA is mainly reflected in Equation (6). In short, the aim was to improve its performance in the stage of convergence towards the candidate agent. Due to the randomness of chaotic mapping, the Chaotic-Lévy flight generates a more diverse population that jumps out of the local optimal solution. The convergence stage formula after introducing the Chaotic-Lévy flight strategy is shown as:

$$X(t) = \begin{cases} chaos(t) * levy. * \left(X_{best} - \vec{A} \cdot \vec{PD} \right), & \text{if } r_{rand} < 0.5 \\ chaos(t) * levy. * \left(X_{best} + \vec{A} \cdot \vec{PD} \right), & \text{if } r_{rand} \geq 0.5 \end{cases} \quad (26)$$

where t indicates that the current iteration number belongs to the t -th generation; $chaos(t)$ represents the chaotic value generated by the chaotic map in the t -th generation; $levy$ is the step size calculated by Lévy flight strategy; and the meanings of unexplained parameters

are the same as those in Equation (6). Because the TSA search agents have difficulty searching randomly in the search space and have not explored the optimal solution, the algorithm easily falls into a local optimal solution. However, the small step sizes of the Chaotic-Lévy flight strategy make it possible for the search agents to move to a random position near the candidate solution, thus greatly improving the probability that the best solution will be chosen. In addition, the large step sizes of Chaotic-Lévy flight produce mutability, which occasionally enables search agents to appear elsewhere in the search space to explore other promising areas and avoid premature convergence. Moreover, the value between (0, 1) generated by a chaotic map can also prevent search agents from leaving the search space because of long-distance movement. Due to the randomness and non-repeatability of chaotic mapping, the Chaotic-Lévy flight strategy can generate steps at random, which enhances population diversity. Because of the diversity of chaotic maps, choosing a suitable one to combine with Lévy flight will be studied in the next section. The main process of the improved TSA can be summarized in the pseudo-code displayed in Algorithm 1, and the CLTSA process is illustrated in the flow chart in Figure 3, which describes the important steps of the algorithm.

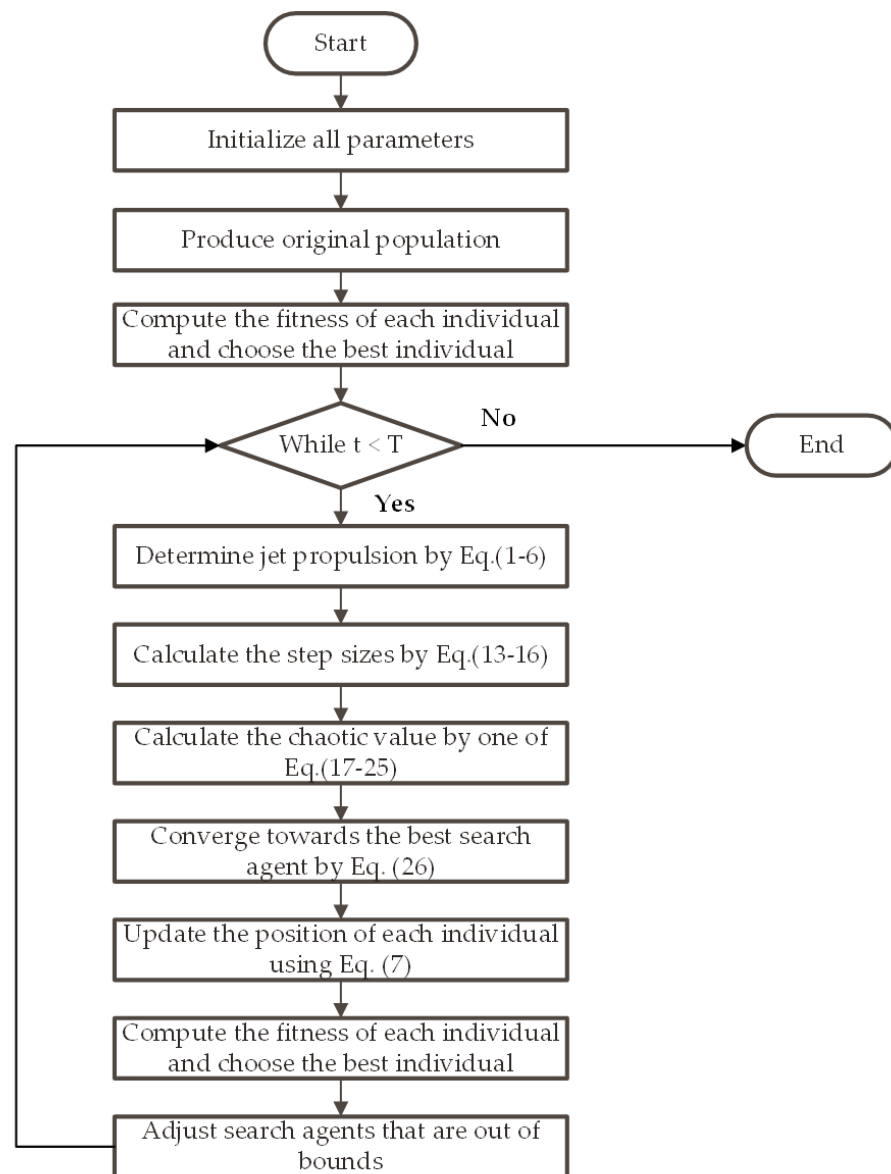


Figure 3. The flowchart of CLTSA.

Algorithm 1: Algorithm CLTSA

```

1: procedure CLTSA
2: Initialize the original population  $\vec{X}$  and the  $chaos(0)$  randomly
3: Initialize the parameters  $\vec{A}$ ,  $\vec{G}$ ,  $\vec{F}$ ,  $\vec{M}$ , and maximum number of iterations T
4: set  $P_{min} \leftarrow 1, P_{max} \leftarrow 4$ 
5: Calculate fitness of each individual, and choose the best candidate solution as  $X_{best}$ 
6:   while ( $t < T$ ) do
7:     for  $i \leftarrow 1$  to  $N$  do
8:       /* Jet propulsion behavior */
9:        $c_1, c_2, c_3, r_{rand} \leftarrow Rand()$ 
10:       $\vec{M} \leftarrow \lfloor P_{min} + c_1 \cdot (P_{max} - P_{min}) \rfloor$  Equation (4)
11:       $\vec{F} \leftarrow 2 \cdot c_1$  Equation (3)
12:       $\vec{G} \leftarrow c_2 + c_3 - \vec{F}$  Equation (2)
13:       $\vec{A} \leftarrow \frac{\vec{G}}{\vec{M}}$  Equation (1)
14:       $\vec{PD} \leftarrow abs\left(\vec{X}_{best} - r_{rand} \cdot \vec{X}(t)\right)$  Equation (5)
15:       $chaos(t) \leftarrow F_{Tent\ map}(chaos(t-1))$  Equation (17)–(25)
16:       $levy \leftarrow F_{levy\ flight}(D)$  Equation (13)–(16)
17:      /* Swarm behavior */
18:      if  $i = 1$ 
19:        if  $r_{rand} < 0.5$ 
20:           $X_i(t+1) \leftarrow X_{best} - \vec{A} \cdot \vec{PD}$  Equation (6)
21:        else
22:           $X_i(t+1) \leftarrow X_{best} + \vec{A} \cdot \vec{PD}$ 
23:        end if
24:      else
25:        if  $r_{rand} < 0.5$ 
26:           $X_i(t) \leftarrow chaos(t) * levy * \left(X_{best} - \vec{A} \cdot \vec{PD}\right)$  Equation (26)
27:        else
28:           $X_i(t) \leftarrow chaos(t) * levy * \left(X_{best} + \vec{A} \cdot \vec{PD}\right)$ 
29:        end if
30:       $X_i(t+1) \leftarrow \frac{X_i(t) + X_{i-1}(t+1)}{(2+c_1)}$  Equation (7)
31:    end for
32:    Calculate fitness of each individual, and choose the best solution as  $X_{best}$ 
33:     $t \leftarrow t + 1$ 
34:  end while
35: return  $X_{best}$ 
36: end procedure

```

3.5. Complexity Analysis of CLTSA

Complexity is an important indicator for evaluating the performance of an algorithm: time complexity estimates running time, and space complexity represents the amount of solution space required. This subsection evaluates the time and space complexity of the CLTSA.

3.5.1. Time Complexity

In the initialization phase, the algorithm generates the original population containing N search agents for a problem with dimension D , so the time complexity of the initialization is $O(N \times D)$. Moreover, CLTSA requires $O(T \times N \times D)$ time to compute the fitness of each individual, where T indicates the maximum number of iterations. Finally, $O(M)$ time is used to execute the main steps, where M denotes the number of jet propulsion and swarm behaviors. Therefore, the overall time complexity of CLTSA is $O(T \times N \times M \times D)$.

3.5.2. Space Complexity

The number of solution spaces required by CLTSA is N search agents generated for D -dimensional problems in the initialization phase. Hence, the space complexity is estimated to be $O(N \times D)$.

4. Experimental Results and Analysis

In the field of meta-heuristic algorithms, using benchmark functions with different characteristics is the most common method for measuring algorithmic performance. These functions can reflect the convergence speed and value of algorithms to evaluate its exploration and development capabilities. To control the accuracy of the experimental results, each algorithm runs independently 30 times on the same software and computer. The software for coding the proposed algorithm is MATLAB 2020a, and the algorithm was run on a computer with AMD Ryzen 7 4800H processor and 16 GB RAM.

4.1. Benchmark Test Functions

The main characteristics of benchmark function are modality, dimensionality, separability, differentiability, and continuity. According to the above characteristics, benchmark functions can be classified to evaluate the performance of algorithms from different perspectives. To comprehensively assess the property of CLTSA, a set of benchmark functions containing all the above features is used [11]. The test set is divided into two groups based on the number of minimums of benchmark functions in a given interval:

1. Unimodal benchmark functions: The detailed information of the unimodal functions test set is listed in Table 2, and their mathematical expressions are shown in Table A1 in Appendix A [11].
2. Multimodal benchmark functions: The detailed information of the test set which is composed of 14 multimodal benchmark functions is listed in Table 3, and their mathematical expressions are shown in Table A2 in Appendix A [11].

Table 2. Unimodal benchmark functions.

| Function | Range | Dim | F_{min} |
|----------------------|---------------|-----|-----------|
| F1-Sphere | [−100, 100] | 50 | 0 |
| F2-Quartic Noise | [−1.28, 1.28] | 20 | 0 |
| F3-Powell Sum | [−1, 1] | 50 | 0 |
| F4-Schwefel's 2.20 | [−100, 100] | 50 | 0 |
| F5-Schwefel's 2.21 | [−100, 100] | 50 | 0 |
| F6-Schwefel's 1.20 | [−100, 100] | 50 | 0 |
| F7-Schwefel's 2.22 | [−100, 100] | 50 | 0 |
| F8-Schwefel's 2.23 | [−10, 10] | 50 | 0 |
| F9-RosenBrock | [−30, 30] | 50 | 0 |
| F10-Brown | [−1, 4] | 50 | 0 |
| F11-Dixon and Price | [−10, 10] | 50 | 0 |
| F12-Powell Singular | [−4, 5] | 50 | 0 |
| F13-Zakharow | [−5, 10] | 50 | 0 |
| F14-Three-Hump Camel | [−5, 5] | 2 | 0 |
| F15-Matyas | [−10, 10] | 2 | 0 |
| F16-WayBurn Seader 3 | [−500, 500] | 2 | 21.35 |

4.2. Comparison of Chaotic Maps

The logistic map is used by most optimization algorithms based on the chaos mechanism in current research [58], but its chaotic values are generally distributed in the intervals $[0, 0.1]$ and $[0.9, 1]$. This uneven traversal affects the optimization efficiency of the algorithm [43]. To select the most suitable chaotic map, the above nine common chaotic maps are combined with the Lévy flight strategy to optimize the TSA. Then, the 30 well-known unimodal test functions and multi-modal test functions (see the Appendix A) are used to evaluate the algorithm's performance. The run results are shown in Tables 4 and 5.

Table 4. Cont.

| Fn | Criteria | Chebyshev | Circle | Gauss | Iterative | Logistic | Sine | Singer | Sinusoidal | Tent |
|-----|----------|-----------|----------|----------|-----------|----------|----------|----------|------------|-----------------|
| F14 | Mean | 0.00E+00 | 0.00E+00 | 0.00E+00 | 0.00E+00 | 0.00E+00 | 0.00E+00 | 0.00E+00 | 0.00E+00 | 0.00E+00 |
| | Best | 0.00E+00 | 0.00E+00 | 0.00E+00 | 0.00E+00 | 0.00E+00 | 0.00E+00 | 0.00E+00 | 0.00E+00 | 0.00E+00 |
| | Std | 0.00E+00 | 0.00E+00 | 0.00E+00 | 0.00E+00 | 0.00E+00 | 0.00E+00 | 0.00E+00 | 0.00E+00 | 0.00E+00 |
| F15 | Mean | 0.00E+00 | 0.00E+00 | 0.00E+00 | 0.00E+00 | 0.00E+00 | 0.00E+00 | 0.00E+00 | 0.00E+00 | 0.00E+00 |
| | Best | 0.00E+00 | 0.00E+00 | 0.00E+00 | 0.00E+00 | 0.00E+00 | 0.00E+00 | 0.00E+00 | 0.00E+00 | 0.00E+00 |
| | Std | 0.00E+00 | 0.00E+00 | 0.00E+00 | 0.00E+00 | 0.00E+00 | 0.00E+00 | 0.00E+00 | 0.00E+00 | 0.00E+00 |
| F16 | Mean | 1.91E+01 | 1.91E+01 | 1.91E+01 | 1.92E+01 | 1.49E+02 | 1.91E+01 | 1.91E+01 | 1.49E+02 | 1.91E+01 |
| | Best | 1.91E+01 | 1.91E+01 | 1.91E+01 | 1.91E+01 | 1.91E+01 | 1.91E+01 | 1.91E+01 | 1.91E+01 | 1.91E+01 |
| | Std | 1.54E−02 | 1.63E−02 | 1.82E−02 | 1.56E−02 | 9.88E+01 | 1.76E+02 | 2.17E−02 | 2.37E+01 | 1.30E−02 |

Table 5. Results of 9 chaotic maps combined with Lévy flight on multimodal benchmark functions.

| Fn | Criteria | Chebyshev | Circle | Gauss | Iterative | Logistic | Sine | Singer | Sinusoidal | Tent |
|-----|----------|------------------|------------------|------------------|------------------|------------------|------------------|------------------|------------------|------------------|
| F17 | Mean | 0.00E+00 |
| | Best | 0.00E+00 |
| | Std | 0.00E+00 |
| F18 | Mean | 9.00E−01 | 1.26E+01 | 9.00E−01 | 9.00E−01 | 9.00E−01 | 9.00E−01 | 9.00E−01 | 9.00E−01 | 9.00E−01 |
| | Best | 9.00E−01 | 1.13E+01 | 9.00E−01 | 9.00E−01 | 9.00E−01 | 9.00E−01 | 9.00E−01 | 9.00E−01 | 9.00E−01 |
| | Std | 8.46E−16 | 5.64E−01 | 3.64E−16 | 8.49E−16 | 4.92E−16 | 3.77E−16 | 7.31E−16 | 6.97E−16 | 4.52E−16 |
| F19 | Mean | 1.91E−231 | 2.58E−211 | 0.00E+00 | 5.57E−182 | 0.00E+00 | 0.00E+00 | 0.00E+00 | 0.00E+00 | 0.00E+00 |
| | Best | 7.41E−234 | 1.89E−218 | 0.00E+00 | 3.14E−182 | 0.00E+00 | 0.00E+00 | 0.00E+00 | 0.00E+00 | 0.00E+00 |
| | Std | 0.00E+00 | 0.00E+00 | 0.00E+00 | 0.00E+00 | 0.00E+00 | 0.00E+00 | 0.00E+00 | 0.00E+00 | 0.00E+00 |
| F20 | Mean | 0.00E+00 | 1.93E−218 | 0.00E+00 |
| | Best | 0.00E+00 | 3.76E−260 | 0.00E+00 |
| | Std | 0.00E+00 | 1.11E−57 | 0.00E+00 |
| F21 | Mean | −8.88E−16 |
| | Best | −8.88E−16 |
| | Std | 0.00E+00 |
| F22 | Mean | 1.49E+02 | 1.48E+02 | 1.61E+02 | 1.54E+02 | 1.63E+02 | 1.48E+02 | 1.61E+02 | 1.46E+02 | 1.53E+02 |
| | Best | 1.42E+02 | 1.38E+02 | 1.38E+02 | 1.28E+02 | 1.23E+02 | 1.29E+02 | 1.37E+02 | 1.36E+02 | 1.30E+02 |
| | Std | 4.81E+01 | 6.50E+00 | 7.57E+00 | 6.99E+00 | 4.81E+01 | 4.95E+01 | 7.94E+00 | 7.82E+00 | 9.19E+00 |
| F23 | Mean | 0.00E+00 | 1.79E−145 | 0.00E+00 | 3.98E−153 | 0.00E+00 | 0.00E+00 | 0.00E+00 | 0.00E+00 | 0.00E+00 |
| | Best | 0.00E+00 | 0.00E+00 | 0.00E+00 | 0.00E+00 | 0.00E+00 | 0.00E+00 | 0.00E+00 | 0.00E+00 | 0.00E+00 |
| | Std | 1.82E−02 | 5.07E−02 | 0.00E+00 | 3.79E−02 | 0.00E+00 | 0.00E+00 | 1.82E−02 | 0.00E+00 | 0.00E+00 |
| F24 | Mean | 0.00E+00 |
| | Best | 0.00E+00 |
| | Std | 0.00E+00 |
| F25 | Mean | 4.90E+00 | 4.73E+00 | 4.90E+00 | 4.80E+00 | 4.99E+00 | 4.99E+00 | 4.90E+00 | 4.90E+00 | 4.88E+00 |
| | Best | 4.51E+00 | 4.35E+00 | 4.80E+00 | 4.53E+00 | 4.84E+00 | 4.98E+00 | 4.80E+00 | 4.80E+00 | 4.70E+00 |
| | Std | 9.90E−02 | 9.85E−02 | 4.02E−02 | 8.54E−02 | 3.79E−02 | 4.82E−03 | 4.13E−02 | 3.29E−02 | 4.34E−02 |
| F26 | Mean | 9.11E−01 | 7.47E−01 | 9.93E−01 | 5.76E−01 | 1.29E+00 | 1.05E+00 | 7.85E−01 | 1.06E+00 | 9.19E−01 |
| | Best | 6.94E−01 | 6.08E−01 | 5.60E−01 | 5.48E−01 | 4.82E−01 | 4.23E−01 | 6.39E−01 | 6.59E−01 | 5.23E−01 |
| | Std | 1.11E−01 | 1.68E−01 | 1.54E−01 | 1.56E−01 | 2.80E−01 | 2.09E−01 | 1.30E−01 | 2.04E−01 | 1.89E−01 |
| F27 | Mean | 0.00E+00 |
| | Best | 0.00E+00 |
| | Std | 0.00E+00 |
| F28 | Mean | −106.722 | −106.727 | −106.73 | −106.74 | −87.3035 | −106.619 | −106.688 | −106.716 | −106.748 |
| | Best | −106.764 | −106.763 | −106.764 | −106.764 | −106.764 | −106.761 | −106.763 | −106.764 | −106.763 |
| | Std | 4.04E−02 | 5.28E−02 | 2.12E−02 | 4.33E−02 | 8.37E+00 | 6.71E+00 | 7.75E−02 | 3.42E−02 | 2.57E−02 |
| F29 | Mean | 3.00E+00 | 3.00E+00 | 3.00E+00 | 3.00E+00 | 3.00E+00 | 3.01E+00 | 3.00E+00 | 3.00E+00 | 3.00E+00 |
| | Best | 3.00E+00 | 3.00E+00 |
| | Std | 2.23E−05 | 3.53E−04 | 5.85E−05 | 1.13E−05 | 6.85E+00 | 1.60E+01 | 3.69E−04 | 1.78E−04 | 9.53E−16 |
| F30 | Mean | 8.23E−02 | 1.19E−01 | 7.87E−02 | 9.06E−02 | 5.93E+01 | 8.97E−01 | 6.00E+01 | 6.45E−03 | 8.59E+00 |
| | Best | 3.17E−02 | 2.30E−02 | 3.83E−02 | 2.30E−02 | 1.56E−02 | 1.85E−02 | 5.16E−03 | 2.76E−03 | 8.49E−03 |
| | Std | 1.50E+01 | 1.46E+00 | 4.24E+01 | 9.77E−01 | 4.80E+01 | 5.73E+01 | 1.81E+01 | 1.50E+01 | 2.03E+01 |

To ensure the fairness and validity of the experimental results, each Chaotic-Lévy TSA was run 30 times independently, and the maximum number of iterations, population size,

and problem dimension were set to 500, 50, and 50 respectively. The mean was the mean value of the 30 optimal solutions. Best was the optimal value among the experimental results obtained by running an algorithm 30 times; std was standard deviation. In this paper, the ranking rule of algorithm performance was mean, best, and std in that order. The algorithm with the best results for each benchmark function is emphasized in bold.

From the experimental results, the Tent-Lévy flight TSA (TLTSA) had far better optimization compared to the Chaotic-Lévy TSAs (CLTSAs). Among the 30 benchmark functions, the TLTSA had 25 optimal solutions more than the CLTSAs and ranked first. In the following research, it was used for comparative experiments and to optimize solutions to engineering problems.

4.3. Parameter Settings of TLTSA and Other Algorithms

The TSA relies on two main parameters to build social interactions, P_{min} and P_{max} . P_{min} was taken as 1, 2, 3, 4 for the experiment and other parameter settings were kept unchanged. The study found that the TSA achieved the best performances when the value of P_{min} was set to 1. In the same way, P_{max} was taken as 1, 2, 3, 4 for the experiment and the other parameter settings were kept unchanged. The TSA achieved the best performances when the value of P_{max} was set to 4 [45]. The proposed TLTSA was compared with TSA and other metaheuristic algorithms, including grey wolf optimizer (GWO) [61], sine cosine algorithm (SCA) [62], sparrow search algorithm (SSA) [63], water circle algorithm (WCA) [8], whale optimization algorithm (WOA) [24], marine predators algorithm (MPA) [64], lighting search algorithm (LSA) [28], and hybrid glowworm swarm optimization (HGSO) [65]. The parameter settings of all algorithms are listed in Table 6, and all parameter values were derived from the literature.

Table 6. The main parameter settings of the algorithms that need to be compared and analyzed.

| Algorithm | Parameter Setting |
|-----------------|--|
| Common Settings | Population size: $N = 50$ maximum number of iterations: $T = 500$ Dimensions of problem: $Dim = 50$ Number of independent runs: $Repetition = 30$ |
| GWO | \vec{a} decays from 2 to 0 \vec{A}, \vec{C} are calculated by corresponding formulas |
| SCA | $a = 2$, $r_{1,2,3,4}$ are calculated by corresponding formulas |
| SSA | Q is a random number and $Q \sim N(\mu, \sigma^2)$ β is a random number and $\beta \sim N(0, 1)$ |
| WCA | $C = 2$ and $\mu = 0.1$ |
| WOA | $\vec{\alpha}$ decays from 2 to 0 $b = 1$ |
| MPA | $p = 0.5$, $FADs = 0.2$ CF is calculated by corresponding formulas |
| LSA | Channel time: $ch_{time} = 10$ |
| HGSO | $\rho = 0.4$, $\gamma = 0.6$, $\beta = 0.08$, $s = 0.03$, $CR = 0.9$, $\lambda = 0.9415$ |
| TSA | $P_{min} = 1$ and $P_{max} = 4$ |
| TLTSA | $P_{min} = 1$ and $P_{max} = 4$ $lévy$ and $chaos(t)$ are calculated by corresponding formulas |

4.4. Results and Analysis

4.4.1. Experimental Data Analysis

Since a fixed-dimensional function is closer to a real-world optimization problem, six were selected to verify TL TSA convergence speed and accuracy. These functions are listed in Table 7, and the mathematical expressions are detailed in Table A3 in the Appendix A.

Table 7. Fixed-dimension benchmark functions.

| Function | Range | Dim | F_{min} |
|----------------------|-----------|-----|-----------|
| F1-Shekel's Foxholes | [−65, 65] | 2 | 1 |
| F2-Kowalik | [−5, 5] | 4 | 0.0003075 |
| F3-Hartman 3 | [0, 1] | 4 | −3.86 |
| F4-Shekel 1 | [0, 10] | 4 | −10.1532 |
| F5-Shekel 2 | [0, 10] | 4 | −10.4029 |
| F6-Shekel 3 | [0, 10] | 4 | −10.5364 |

Because unimodal benchmark functions have only one global minimum, it is not only suitable for assessing development capability, but also for examining the algorithm convergence speed. According to the experimental data in Table 8, the TL TSA was more competitive in the unimodal benchmark functions compared to other algorithms. For F1, F3, F4, F5, F6, and F7, only the TL TSA quickly and accurately found the standard optimal value 0. In addition, the std was also zero, which showed that running TL TSA 30 times produced the best global solution and fully reflected its stability. For the other algorithms, it was difficult for them to find the global optimal solution with an order of magnitude less than −100, especially the SCA, SSA, and LSA. These three converged prematurely because they could not escape the local optimal solution. For F10, F12, F13, F14, and F15, although some of the other comparison algorithms also had good performance, there was still a large gap with the TL TSA, which quickly found the exact global optimal solution. For these unimodal benchmark functions, the order of magnitude of the mean value of the HGSO reached −100 even −200, and the std reached 0. However, the mean, best, and std of the TL TSA were all zero, which meant that the TL TSA had strong optimization capability and stability. From the comparison of these three criteria, it more carefully developed the vicinity of the optimal solution than did the HGSO, thereby enhancing the selectivity of the optimal solution. For F2, F9, and F11, although the best result of TL TSA is not optimal solution 0, it has the best mean value, optimal solution, and std among the algorithms selected for comparison. It was proven that the proposed TL TSA was indeed focused on exploration and exploitation to improve performance. For F8, although both the TL TSA and HGSO had the best calculation accuracy, the convergence curve indicates that the convergence speed of TL TSA was significantly better, showing that it has more exploration and exploitation advantages. For F16, TL TSA obtains the same global optimal solution as the other algorithms, but was slightly unstable. In addition, compared with the original TSA algorithm, the TL TSA had a greatly improved mean value and standard deviation as well as a high-er search accuracy. Overall, in the test of 16 unimodal benchmark functions, the TL TSA took first place 15 times and eighth once among 10 algorithms.

It was clearly better suited to solving precise engineering problems, and its higher sensitivity to unimodal benchmark functions proved a strong exploitation capability. The Tent-Lévy flight strategy generated a number of small step sizes with greater randomness, which made search agents explore the search space fully when converging towards the candidate solution, and improve the possibility of the optimal solution being selected. Tent-Lévy flight as a random-walk strategy efficiently enhanced the algorithm's exploration and exploitation abilities.

Table 8. Comparison of TL TSA with other optimization algorithms for unimodal benchmark functions.

| Fn | Criteria | GWO | SCA | SSA | WCA | WOA | MPA | LSA | HGSO | LFPSO [47] | chTLBO [66] | TSA | TL TSA |
|-----|----------|-----------|----------|----------|----------|-----------|-----------------|-----------|-----------------|------------|-----------------|-----------|-----------------|
| F1 | Mean | 8.11E−24 | 5.78E+02 | 2.35E−03 | 9.98E−10 | 4.43E−83 | 5.10E−21 | 1.13E−04 | 4.52E−114 | 1.06E−04 | 7.32E−05 | 9.65E−18 | 0.00E+00 |
| | Best | 5.29E−25 | 2.13E+00 | 6.05E−05 | 6.97E−14 | 9.90E−93 | 6.88E−23 | 7.36E−08 | 6.97E−150 | — | 1.45E−06 | 7.93E−20 | 0.00E+00 |
| | Std | 1.10E−23 | 7.67E+02 | 2.17E−03 | 2.33E−09 | 2.19E−82 | 7.53E−21 | 3.07E−04 | 2.48E−113 | 1.58E−04 | — | 1.40E−17 | 0.00E+00 |
| F2 | Mean | 2.12E−03 | 2.16E+00 | 3.41E−01 | 3.78E−02 | 2.55E−03 | 1.32E−03 | 7.88E−02 | 2.47E−04 | 4.34E−02 | 1.63E−01 | 1.14E−02 | 4.03E−05 |
| | Best | 8.10E−04 | 1.54E−01 | 1.67E−01 | 2.12E−02 | 1.34E−05 | 2.63E−04 | 5.21E−02 | 1.69E−05 | — | 7.61E−02 | 2.55E−03 | 7.99E−07 |
| | Std | 9.10E−04 | 2.55E+00 | 8.43E−02 | 1.26E−02 | 3.17E−03 | 6.51E−04 | 1.44E−02 | 2.46E−04 | 1.11E−02 | — | 4.85E−03 | 4.00E−05 |
| F3 | Mean | 3.54E−107 | 6.52E−03 | 7.77E−07 | 2.23E−22 | 7.09E−124 | 8.98E−62 | 8.36E−32 | 5.16E−207 | — | — | 1.14E−75 | 0.00E+00 |
| | Best | 1.13E−118 | 1.56E−04 | 4.63E−08 | 6.84E−29 | 3.47E−153 | 5.70E−72 | 1.21E−39 | 1.45E−234 | — | — | 6.46E−92 | 0.00E+00 |
| | Std | 1.53E−106 | 1.15E−02 | 8.57E−07 | 7.45E−22 | 3.88E−123 | 3.66E−61 | 4.52E−31 | 0.00E+00 | — | — | 3.67E−75 | 0.00E+00 |
| F4 | Mean | 1.10E−13 | 2.52E+00 | 4.22E+01 | 1.29E−04 | 8.52E−53 | 2.70E−11 | 7.13E−01 | 5.68E−71 | — | — | 1.25E−10 | 0.00E+00 |
| | Best | 7.13E−14 | 7.05E−02 | 1.27E+01 | 1.42E−05 | 3.87E−58 | 3.05E−12 | 3.24E−03 | 2.94E−75 | — | — | 4.08E−11 | 0.00E+00 |
| | Std | 3.95E−14 | 2.33E+00 | 2.47E+01 | 2.51E−04 | 2.54E−52 | 1.78E−11 | 8.78E−01 | 8.55E−71 | — | — | 8.80E−11 | 0.00E+00 |
| F5 | Mean | 5.80E−05 | 6.33E+01 | 1.58E+01 | 2.98E+00 | 8.14E+01 | 2.93E−08 | 1.64E+01 | 3.03E−66 | 1.21E+01 | 2.10E−03 | 4.62E+00 | 0.00E+00 |
| | Best | 5.88E−06 | 4.21E+01 | 1.39E+01 | 8.40E−01 | 6.45E+01 | 1.52E−08 | 9.02E+00 | 2.73E−73 | — | 2.10E−03 | 6.55E−01 | 0.00E+00 |
| | Std | 6.34E−05 | 1.01E+01 | 1.61E+00 | 9.16E−01 | 9.43E+00 | 1.01E−08 | 7.42E−66 | 6.22E+00 | — | — | 2.84E+00 | 0.00E+00 |
| F6 | Mean | 5.43E−03 | 3.91E+04 | 4.64E+03 | 7.44E+00 | 1.52E+05 | 1.86E−02 | 2.84E+03 | 4.34E−126 | 1.18E+03 | 1.84E−02 | 2.11E+00 | 0.00E+00 |
| | Best | 3.01E−06 | 1.42E+04 | 1.46E+03 | 2.36E+00 | 7.99E+04 | 2.79E−04 | 1.25E+03 | 4.94E−144 | — | 1.30E−03 | 8.37E−03 | 0.00E+00 |
| | Std | 1.14E−02 | 1.50E+04 | 3.18E+03 | 4.92E+00 | 3.20E+04 | 2.74E−02 | 6.87E+02 | 2.31E−125 | 5.66E+02 | — | 3.51E+00 | 0.00E+00 |
| F7 | Mean | 2.02E−13 | 3.64E+00 | 6.49E+28 | 1.74E+25 | 6.01E−53 | 2.79E−11 | 1.21E+02 | 1.19E−66 | 1.73E−03 | 1.00E−02 | 1.99E−10 | 0.00E+00 |
| | Best | 7.59E−14 | 1.44E−01 | 6.69E+08 | 7.88E−07 | 6.42E−59 | 5.29E−13 | 2.30E−01 | 1.58E−75 | — | 1.61E−01 | 2.70E−12 | 0.00E+00 |
| | Std | 9.92E−14 | 4.69E+00 | 3.35E+29 | 9.54E+25 | 2.97E−52 | 4.13E−11 | 1.47E+02 | 6.34E−66 | 4.53E−03 | — | 1.89E−10 | 0.00E+00 |
| F8 | Mean | 6.74E−77 | 1.13E+08 | 1.13E−03 | 2.14E−25 | 9.77E−226 | 4.43E−94 | 1.68E−18 | 0.00E+00 | — | — | 3.87E−42 | 0.00E+00 |
| | Best | 2.32E−85 | 4.09E+06 | 8.06E−08 | 1.51E−34 | 3.93E−293 | 2.50E−101 | 6.12E−24 | 0.00E+00 | — | — | 3.46E−59 | 0.00E+00 |
| | Std | 2.48E−76 | 1.50E+08 | 3.16E−03 | 1.13E−24 | 0.00E+00 | 1.52E−93 | 4.90E−18 | 0.00E+00 | — | — | 1.84E−41 | 0.00E+00 |
| F9 | Mean | 4.66E+01 | 5.12E+06 | 4.55E+02 | 9.41E+01 | 4.76E+01 | 4.88E+01 | 1.45E+02 | 4.88E+01 | 9.78E+01 | 1.99E+01 | 4.87E+01 | 4.54E+01 |
| | Best | 4.58E+01 | 2.00E+05 | 8.01E+01 | 4.32E+01 | 4.68E+01 | 4.81E+01 | 2.98E+01 | 4.87E+01 | — | 1.86E+01 | 4.85E+01 | 4.48E+01 |
| | Std | 5.25E−01 | 6.33E+06 | 7.95E+02 | 3.62E+01 | 5.00E−01 | 2.57E−01 | 5.99E+01 | 1.02E−01 | 6.53E+01 | — | 1.17E−01 | 4.92E−01 |
| F10 | Mean | 2.30E−26 | 2.11E−01 | 6.37E−05 | 1.33E−13 | 1.46E−87 | 8.85E−24 | 2.62E−05 | 7.86E−136 | — | — | 5.73E−20 | 0.00E+00 |
| | Best | 1.26E−27 | 2.93E−03 | 4.30E−07 | 7.28E−17 | 5.40E−96 | 8.02E−25 | 2.01E−09 | 6.09E−160 | — | — | 3.01E−22 | 0.00E+00 |
| | Std | 3.23E−26 | 3.43E−01 | 2.40E−04 | 2.72E−13 | 4.77E−87 | 7.70E−24 | 6.42E−05 | 3.82E−135 | — | — | 1.16E−19 | 0.00E+00 |
| F11 | Mean | 6.67E−01 | 2.26E+04 | 1.30E+01 | 6.67E−01 | 6.67E−01 | 6.67E−01 | 6.05E+00 | 6.67E−01 | — | — | 7.56E−01 | 6.67E−01 |
| | Best | 6.67E−01 | 1.77E+02 | 1.80E+00 | 6.67E−01 | 6.67E−01 | 6.67E−01 | 1.03E+00 | 6.67E−01 | — | — | 6.67E−01 | 6.67E−01 |
| | Std | 1.41E−05 | 3.49E+04 | 1.38E+01 | 3.83E−04 | 1.87E−04 | 8.56E−08 | 3.35E+00 | 2.87E−06 | — | — | 1.50E−01 | 4.32E−08 |
| F12 | Mean | 1.63E−05 | 2.24E+02 | 9.05E+00 | 1.10E−03 | 9.15E−13 | 2.08E−15 | 4.20E−01 | 8.34E−116 | — | — | 5.15E−04 | 0.00E+00 |
| | Best | 2.27E−06 | 2.64E+00 | 1.08E+00 | 3.03E−04 | 5.82E−95 | 5.71E−23 | 5.57E−02 | 1.93E−150 | — | — | 8.95E−05 | 0.00E+00 |
| | Std | 1.09E−05 | 2.32E+02 | 6.07E+00 | 4.65E−04 | 4.84E−12 | 1.13E−14 | 5.10E−01 | 4.57E−115 | — | — | 4.46E−04 | 0.00E+00 |
| F13 | Mean | 8.68E−05 | 1.28E+02 | 2.60E+02 | 1.75E+02 | 8.52E+02 | 1.70E−01 | 1.09E+02 | 1.85E−119 | — | — | 1.27E−06 | 0.00E+00 |
| | Best | 4.11E−07 | 5.14E+01 | 1.55E+02 | 2.86E+01 | 5.96E+02 | 4.60E−02 | 6.30E+01 | 1.81E−138 | — | — | 1.67E−08 | 0.00E+00 |
| | Std | 1.03E−04 | 4.94E+01 | 6.69E+01 | 7.29E+01 | 1.09E+02 | 9.01E−02 | 2.18E+01 | 9.73E−119 | — | — | 2.30E−06 | 0.00E+00 |
| F14 | Mean | 1.89E−240 | 8.74E−78 | 3.49E−15 | 1.45E−39 | 1.45E−95 | 7.53E−80 | 5.67E−253 | 9.51E−183 | — | — | 2.99E−02 | 0.00E+00 |
| | Best | 1.39E−307 | 5.19E−87 | 2.81E−18 | 9.77E−45 | 9.31E−119 | 1.42E−119 | 1.88E−263 | 4.51E−220 | — | — | 4.96E−150 | 0.00E+00 |
| | Std | 0.00E+00 | 3.35E−77 | 4.60E−15 | 4.31E−39 | 6.62E−95 | 4.12E−79 | 0.00E+00 | 0.00E+00 | — | — | 9.11E−02 | 0.00E+00 |
| F15 | Mean | 2.45E−140 | 5.74E−61 | 8.63E−16 | 1.91E−40 | 2.15E−213 | 1.04E−70 | 1.60E−149 | 1.39E−181 | — | — | 1.25E−86 | 0.00E+00 |
| | Best | 1.23E−165 | 2.56E−79 | 4.10E−18 | 3.89E−46 | 1.09E−270 | 1.25E−90 | 5.17E−171 | 5.05E−213 | — | — | 3.25E−101 | 0.00E+00 |
| | Std | 1.29E−139 | 3.14E−60 | 1.05E−15 | 4.12E−40 | 0.00E+00 | 5.68E−70 | 8.64E−149 | 0.00E+00 | — | — | 5.64E−86 | 0.00E+00 |
| F16 | Mean | 1.91E+01 | 1.91E+01 | 1.91E+01 | 1.91E+01 | 1.91E+01 | 1.91E+01 | 1.91E+01 | 1.93E+01 | — | — | 6.80E+01 | 1.91E+01 |
| | Best | 1.91E+01 | 1.91E+01 | 1.91E+01 | 1.91E+01 | 1.91E+01 | 1.91E+01 | 1.91E+01 | 1.91E+01 | — | — | 1.91E+01 | 1.91E+01 |
| | Std | 1.03E−05 | 2.15E−02 | 2.86E−10 | 9.49E−15 | 3.61E−03 | 5.15E−15 | 1.35E−14 | 1.85E−01 | — | — | 1.24E+02 | 3.71E−02 |

Table 9 is the experimental data of multimodal benchmark functions. A significant characteristic of the multimodal benchmark functions is that they may have multiple local minimum values in a given interval, so the multimodal benchmark functions are important tools to evaluate the global search capability of optimization algorithms. For F18, F19, F20, F23, F27, and F29, the three statistics of TL TSA are all better than other comparison algorithms, which means that TL TSA can always easily jump out of the local optimal value and concentrate on finding the global optimal solution. It can be seen that TL TSA ranks first in each group. For F17, F21, and F24, the optimization effect of mean, best, and std of TL TSA is obvious. The proposed TL TSA enhances the global exploration capability on the basis of TSA and solves the premature convergence problem, tied for first place with some algorithms in each group. For F22 and F25, the mean of TL TSA is better than SCA, SSA, HGSO, and TSA, which demonstrates that TL TSA makes progress on exploring in search space. For F26, F28, and F30, the performance of TL TSA is greatly ameliorated compared

with TSA, which makes TL TSA more competitive. Through the above experimental results analysis, it is shown that TL TSA has enough global exploration capability to escape from the local optimal solution. The ergodicity and randomness of the Tent map promote the search agents to distribute in search space randomly, which improves the diversity of the population. In addition, when the Tent-Lévy flight strategy executes random walk, the large step sizes are generated with a certain probability, which enables TL TSA to effectively search for possible areas in the space.

Table 9. Comparison of TL TSA with other optimization algorithms for multimodal benchmark functions.

| Fn | Criteria | GWO | SCA | SSA | WCA | WOA | MPA | LSA | HGSO | LFP SO [47] | chTLBO [66] | TSA | TL TSA |
|-----|----------|-----------|----------|----------|-----------------|-----------------|-----------------|-----------------|-----------------|-------------|-----------------|-----------|-----------------|
| F17 | Mean | 3.27E+00 | 1.05E+02 | 7.11E+01 | 8.48E+01 | 0.00E+00 | 0.00E+00 | 1.22E+02 | 0.00E+00 | 2.96E+01 | 3.58E+02 | 3.72E+02 | 0.00E+00 |
| | Best | 5.68E−14 | 1.35E+01 | 3.28E+01 | 5.57E+01 | 0.00E+00 | 0.00E+00 | 7.36E+01 | 0.00E+00 | — | 3.48E+02 | 2.32E+02 | 0.00E+00 |
| | Std | 3.98E+00 | 6.25E+01 | 1.89E+01 | 2.74E+01 | 0.00E+00 | 0.00E+00 | 2.33E+01 | 0.00E+00 | 4.29E+00 | — | 7.09E+01 | 0.00E+00 |
| F18 | Mean | 1.67E+00 | 1.25E+01 | 1.00E+00 | 1.00E+00 | 1.24E+00 | 1.08E+00 | 1.00E+00 | 9.03E−01 | — | — | 8.73E+00 | 9.00E−01 |
| | Best | 1.17E+00 | 9.76E+00 | 1.00E+00 | 1.00E+00 | 9.00E−01 | 1.00E+00 | 1.00E+00 | 9.00E−01 | — | — | 6.64E+00 | 9.00E−01 |
| | Std | 3.77E−01 | 1.13E+00 | 7.12E−05 | 1.60E−11 | 8.27E−01 | 6.78E−02 | 1.67E−03 | 1.75E−02 | — | — | 1.13E+00 | 4.52E−16 |
| F19 | Mean | 7.42E−04 | 6.62E+00 | 5.63E+00 | 2.06E−04 | 5.67E−55 | 5.95E−13 | 3.78E−01 | 7.13E−71 | — | — | 5.87E+01 | 0.00E+00 |
| | Best | 9.42E−14 | 6.05E−02 | 1.38E+00 | 5.13E−09 | 2.22E−60 | 2.22E−14 | 3.98E−03 | 1.58E−79 | — | — | 3.07E+01 | 0.00E+00 |
| | Std | 8.85E−04 | 5.37E+00 | 2.14E+00 | 7.50E−04 | 2.18E−54 | 5.64E−13 | 4.70E−01 | 1.80E−70 | — | — | 1.10E+01 | 0.00E+00 |
| F20 | Mean | 1.38E−20 | 1.04E+09 | 2.58E+01 | 9.62E−05 | 5.06E−03 | 5.91E−16 | 2.44E−08 | 4.94E−73 | — | — | 4.74E−01 | 0.00E+00 |
| | Best | 1.14E−45 | 8.95E−01 | 7.61E−02 | 1.38E−09 | 2.96E−36 | 1.06E−27 | 2.13E−13 | 1.14E−113 | — | — | 3.30E−03 | 0.00E+00 |
| | Std | 7.57E−20 | 3.40E+09 | 6.00E+01 | 5.15E−04 | 2.72E−02 | 3.18E−15 | 6.38E−08 | 2.70E−72 | — | — | 1.13E+00 | 0.00E+00 |
| F21 | Mean | 5.35E−13 | 1.87E+01 | 3.33E+00 | 4.23E−01 | 2.43E−15 | 1.03E−11 | 3.56E+00 | −8.88E−16 | 2.99E−02 | 5.62E−02 | 1.66E+00 | −8.88E−16 |
| | Best | 2.51E−13 | 3.34E+00 | 2.01E+00 | 7.13E−07 | −8.88E−16 | 5.71E−13 | 2.20E+00 | −8.88E−16 | — | 5.12E−02 | 1.75E−10 | −8.88E−16 |
| | Std | 1.80E−13 | 4.88E+00 | 6.61E−01 | 8.73E−01 | 2.79E−15 | 5.17E−12 | 1.66E+00 | 0.00E+00 | 1.18E−01 | — | 1.59E+00 | 0.00E+00 |
| F22 | Mean | 5.66E+01 | 1.31E+04 | 5.14E+02 | 7.11E+01 | 1.23E+02 | 4.76E+01 | 1.50E+02 | 1.58E+02 | — | — | 2.23E+02 | 1.56E+02 |
| | Best | 3.83E+01 | 8.29E+02 | 3.22E+02 | 9.02E+00 | 6.58E+01 | 3.49E+01 | 5.80E+01 | 1.51E+02 | — | — | 1.49E+02 | 1.35E+02 |
| | Std | 9.32E+00 | 1.88E+04 | 1.36E+02 | 5.04E+01 | 3.22E+01 | 7.42E+00 | 5.00E+01 | 3.13E+00 | — | — | 3.77E+01 | 1.11E+01 |
| F23 | Mean | 2.07E−01 | 3.29E+00 | 3.27E+00 | 9.57E−01 | 1.23E−01 | 1.80E−01 | 1.00E+00 | 1.91E−18 | — | — | 4.80E−01 | 0.00E+00 |
| | Best | 9.99E−02 | 1.30E+00 | 2.20E+00 | 7.00E−01 | 5.97E−44 | 9.99E−02 | 6.00E−01 | 4.03E−69 | — | — | 3.00E−01 | 0.00E+00 |
| | Std | 3.65E−02 | 1.25E+00 | 5.31E−01 | 1.30E−01 | 6.26E−02 | 4.07E−02 | 2.57E−01 | 1.04E−17 | — | — | 7.61E−02 | 0.00E+00 |
| F24 | Mean | 1.04E−03 | 1.17E+00 | 3.54E−02 | 6.97E−03 | 0.00E+00 | 0.00E+00 | 1.20E−02 | 0.00E+00 | 1.13E−02 | 8.21E−07 | 4.91E−03 | 0.00E+00 |
| | Best | 0.00E+00 | 4.15E−01 | 1.24E−02 | 7.18E−13 | 0.00E+00 | 0.00E+00 | 2.37E−10 | 0.00E+00 | — | 1.39E−08 | 0.00E+00 | 0.00E+00 |
| | Std | 4.02E−03 | 3.85E−01 | 1.79E−02 | 1.45E−02 | 0.00E+00 | 0.00E+00 | 1.74E−02 | 0.00E+00 | 1.61E−02 | — | 8.38E−03 | 0.00E+00 |
| F25 | Mean | 1.59E+00 | 2.01E+07 | 5.71E+01 | 3.66E−04 | 4.65E−01 | 6.81E−02 | 1.14E−01 | 4.88E+00 | 1.33E−02 | 5.42E−06 | 5.37E+00 | 4.85E+00 |
| | Best | 9.77E−01 | 4.33E+04 | 2.72E+01 | 4.96E−14 | 1.43E−01 | 6.01E−03 | 5.57E−07 | 4.79E+00 | — | 3.73E−07 | 4.24E+00 | 4.73E+00 |
| | Std | 3.51E−01 | 2.24E+07 | 1.65E+01 | 2.01E−03 | 1.81E−01 | 6.24E−02 | 2.40E−01 | 3.94E−02 | 2.59E−02 | — | 7.47E−01 | 3.87E−02 |
| F26 | Mean | 6.58E−02 | 1.05E+07 | 9.15E+00 | 4.31E−08 | 2.32E−02 | 9.92E−04 | 3.08E−01 | 9.28E−01 | 2.91E−01 | 7.91E−08 | 9.94E+00 | 9.14E−01 |
| | Best | 2.33E−02 | 7.18E+00 | 3.70E+00 | 1.07E−13 | 3.22E−03 | 4.44E−05 | 1.28E−06 | 8.34E−01 | — | 1.61E−09 | 2.96E+00 | 6.08E−01 |
| | Std | 2.21E−02 | 1.42E+07 | 4.52E+00 | 1.38E−07 | 7.11E−02 | 1.30E−03 | 4.67E−01 | 4.81E−02 | 6.59E−01 | — | 4.39E+00 | 1.88E−01 |
| F27 | Mean | 3.14E−261 | 3.05E−76 | 7.12E−14 | 1.40E−38 | 8.54E−141 | 9.38E−93 | 2.03E−258 | 8.73E−183 | — | — | 6.42E−121 | 0.00E+00 |
| | Best | 1.03E−305 | 1.25E−86 | 2.24E−15 | 2.09E−45 | 2.89E−168 | 3.46E−128 | 3.47E−266 | 3.57E−203 | — | — | 9.57E−162 | 0.00E+00 |
| | Std | 0.00E+00 | 1.49E−75 | 6.91E−14 | 4.05E−38 | 4.54E−140 | 5.14E−92 | 0.00E+00 | 0.00E+00 | — | — | 3.44E−120 | 0.00E+00 |
| F28 | Mean | −105.468 | −106.721 | −106.765 | −106.765 | −106.765 | −106.765 | −106.765 | −106.371 | — | — | −104.17 | −106.723 |
| | Best | −106.765 | −106.763 | −106.765 | −106.765 | −106.765 | −106.765 | −106.765 | −106.757 | — | — | −106.765 | −106.764 |
| | Std | 4.94E+00 | 4.72E−02 | 1.05E−12 | 3.75E−14 | 6.76E−06 | 6.92E−14 | 3.73E−14 | 3.95E−01 | — | — | 6.73E+00 | 5.47E−02 |
| F29 | Mean | 3.00E+00 | 3.00E+00 | 3.00E+00 | 3.00E+00 | 3.00E+00 | 3.00E+00 | 3.00E+00 | 3.00E+00 | — | — | 9.30E+00 | 3.00E+00 |
| | Best | 3.00E+00 | 3.00E+00 | 3.00E+00 | 3.00E+00 | 3.00E+00 | 3.00E+00 | 3.00E+00 | 3.00E+00 | — | — | 3.00E+00 | 3.00E+00 |
| | Std | 2.21E−05 | 7.52E−05 | 2.69E−13 | 1.16E−15 | 1.11E−05 | 1.81E−15 | 1.59E−04 | 2.29E−03 | — | — | 1.69E+01 | 8.45E−16 |
| F30 | Mean | 3.16E+01 | 3.10E−01 | 1.97E+00 | 1.27E−05 | 7.90E+00 | 1.27E−05 | 5.92E+00 | 2.99E+00 | — | — | 4.64E+01 | 6.52E+00 |
| | Best | 3.00E−05 | 1.54E−02 | 1.27E−05 | 1.27E−05 | 1.28E−05 | 1.27E−05 | 1.27E−05 | 3.69E−03 | — | — | 9.80E−04 | 1.51E−02 |
| | Std | 3.00E+01 | 2.96E−01 | 1.08E+01 | 0.00E+00 | 2.05E+01 | 4.66E−14 | 1.81E+01 | 3.09E+00 | — | — | 4.90E+01 | 1.80E+01 |

Table 10 depicts the experimental results of the fixed-dimension functions. For F33, the TL TSA always found the optimal solution and kept the std to a minimum. For other functions, it greatly improved solution accuracy compared with the original algorithms and was significantly better than most optimization algorithms, showing that it had sufficient ability to jump out of the local optimal solution. Because fixed-dimensional functions are closer to real-life optimization problems and the TL TSA is competitive at solving them, it showed that it could solve constrained engineering problems.

Table 10. Comparison of TL TSA with other optimization algorithms for fixed-dimension functions.

| Fn | Criteria | GWO | SCA | SSA | WCA | WOA | MPA | LSA | HGSO | LFP SO [47] | chTLBO [66] | TSA | TL TSA |
|-----|----------|-----------------|-----------|-----------|-----------|-----------|-----------------|-----------|-----------|-------------|-------------|-----------|-----------------|
| F31 | Mean | 2.81E+00 | 1.66E+00 | 1.16E+00 | 9.98E−01 | 2.21E+00 | 9.98E−01 | 6.89E+00 | 1.41E+00 | 9.98E−01 | 1.02E+01 | 8.41E+00 | 1.06E+00 |
| | Best | 9.98E−01 | 9.98E−01 | 9.98E−01 | 9.98E−01 | 9.98E−01 | 9.98E−01 | 9.98E−01 | 9.98E−01 | 9.98E−01 | 9.99E+00 | 1.99E+00 | 9.98E−01 |
| | Std | 2.35E+00 | 9.51E−01 | 5.87E−01 | 8.25E−17 | 2.47E+00 | 1.62E−16 | 4.79E+00 | 5.21E−01 | 9.21E−17 | | 4.96E+00 | 2.52E−01 |
| F32 | Mean | 4.20E−03 | 1.07E−03 | 2.12E−03 | 4.30E−04 | 7.26E−04 | 3.07E−04 | 5.93E−04 | 4.82E−04 | 1.18E−03 | 3.61E−02 | 5.87E−03 | 5.08E−04 |
| | Best | 3.07E−04 | 3.83E−04 | 3.08E−04 | 3.07E−04 | 3.15E−04 | 3.07E−04 | 3.07E−04 | 3.41E−04 | | 9.10E−03 | 3.08E−04 | 3.35E−04 |
| | Std | 1.16E−02 | 3.85E−04 | 4.97E−03 | 3.17E−04 | 4.65E−04 | 2.76E−15 | 4.59E−04 | 7.56E−05 | 3.63E−03 | | 8.99E−03 | 1.29E−04 |
| F33 | Mean | −3.86E+00 | −3.85E+00 | −3.86E+00 | −3.86E+00 | −3.86E+00 | −3.86E+00 | −3.86E+00 | −3.85E+00 | −3.86E+00 | −3.60E+00 | −3.86E+00 | −3.86E+00 |
| | Best | −3.86E+00 | −3.86E+00 | −3.86E+00 | −3.86E+00 | −3.86E+00 | −3.86E+00 | −3.86E+00 | −3.86E+00 | −3.86E+00 | −3.69E+00 | −3.86E+00 | −3.86E+00 |
| | Std | 2.37E−03 | 2.39E−03 | 2.94E−13 | 2.61E−15 | 5.39E−03 | 2.71E−15 | 3.49E−03 | 5.98E−03 | 2.66E−15 | | 2.55E−03 | 2.32E−15 |
| F34 | Mean | −9.31E+00 | −3.23E+00 | −8.30E+00 | −3.60E+00 | −8.12E+00 | −1.02E+01 | −7.38E+00 | −3.86E+00 | −8.28E+00 | −6.05E+00 | −6.93E+00 | −8.80E+00 |
| | Best | −1.02E+01 | −7.89E+00 | −1.02E+01 | −5.04E+00 | −1.02E+01 | −1.02E+01 | −1.02E+01 | −1.02E+01 | −1.02E+01 | −6.98E+00 | −1.01E+01 | −1.02E+01 |
| | Std | 1.92E+00 | 1.92E+00 | 2.73E+00 | 1.96E+00 | 2.77E+00 | 3.00E−11 | 2.91E+00 | 9.06E−01 | 2.74E+00 | | 3.04E+00 | 2.28E+00 |
| F35 | Mean | −1.04E+01 | −3.33E+00 | −8.97E+00 | −3.88E+00 | −7.49E+00 | −1.04E+01 | −6.75E+00 | −3.84E+00 | −9.97E+00 | −1.04E+01 | −5.50E+00 | −1.00E+01 |
| | Best | −1.04E+01 | −5.62E+00 | −1.04E+01 | −5.08E+00 | −1.04E+01 | −1.04E+01 | −1.04E+01 | −5.22E+00 | | −1.19E+01 | −1.04E+01 | −1.04E+01 |
| | Std | 8.68E−04 | 1.69E+00 | 2.70E+00 | 1.87E+00 | 3.44E+00 | 3.34E−11 | 3.34E+00 | 5.28E−01 | 1.66E+00 | | 3.01E+00 | 1.35E+00 |
| F36 | Mean | −1.01E+01 | −4.49E+00 | −4.98E+00 | −9.24E+00 | −7.60E+00 | −1.05E+01 | −8.68E+00 | −3.98E+00 | −1.01E+01 | −9.23E+00 | −5.75E+00 | −8.88E+00 |
| | Best | −1.05E+01 | −8.60E+00 | −9.31E+00 | −1.05E+01 | −1.05E+01 | −1.05E+01 | −1.05E+01 | −7.55E+00 | | −1.05E+01 | −1.05E+01 | −1.05E+01 |
| | Std | 1.75E+00 | 1.76E+00 | 1.84E+00 | 2.41E+00 | 3.46E+00 | 3.64E−11 | 3.16E+00 | 8.86E−01 | 1.67E+00 | | 3.63E+00 | 3.10E+00 |

To evaluate the fairness and accuracy of TL TSA, the LFP SO [47], chTLBO [66], TSA-LEO [43], and QLGCTSA [44] were selected for comparison. The experimental data of them came from the original literature. Tables 8–10 show that the TL TSA was superior to LFP SO and chTLBO just using chaotic mapping or Lévy flight. From Table 11, it can be seen that the optimization performance of TL TSA and QLGCTSA was significantly better than that of TSA-LEO because local escape operator was difficult to help search agents explore potential areas. Compared with QLGCTSA, the proposed TL TSA performed better in unimodal functions and was similar in multimodal functions, thus demonstrating that chaotic mapping combined with Lévy flight had a stronger global exploration and development ability. In the proposed TL TSA, a number of search agents executing small-step random walks improved the development ability, and several large-step random walks and chaotic mapping enhanced the global exploration. This method overcame the QLGCTSA’s disadvantage that used too many operators to improve the global exploration ability, resulting in unbalanced exploration and development. Hence, the proposed Tent-Lévy flight strategy is more suitable for algorithms like the TSA, which converged prematurely from a lack of exploration and exploitation ability.

Table 11. Comparison of TL TSA with other improved TSAs for benchmark functions.

| Fn | | F1 | F2 | F5 | F6 | F7 | F9 | F13 | F17 | F21 |
|--------------|------|-----------------|-----------------|-----------------|-----------------|-----------------|-----------------|-----------------|-----------------|-----------------|
| QLGCTSA [44] | Mean | 0.00E+00 | 9.06E−05 | 6.34E−209 | 0.00E+00 | 1.15E−213 | 3.54E−05 | | 0.00E+00 | 8.88E−16 |
| | Best | 0.00E+00 | 7.77E−06 | 3.67E−251 | 0.00E+00 | 7.16E−240 | 9.23E−06 | — | 0.00E+00 | 8.88E−16 |
| | Std | 0.00E+00 | 1.09E−04 | 0.00E+00 | 0.00E+00 | 0.00E+00 | 1.81E−05 | | 0.00E+00 | 0.00E+00 |
| TSA-LEO [43] | Mean | | | | | | 5.80E+02 | 6.44E+04 | 7.07E+02 | 3.31E+04 |
| | Best | | | | | | | | | |
| | Std | | | | | | 7.25E+01 | 8.79E+03 | 3.71E+01 | 2.69E+04 |
| TL TSA | Mean | 0.00E+00 | 4.03E−05 | 0.00E+00 | 0.00E+00 | 0.00E+00 | 4.54E+01 | 0.00E+00 | 0.00E+00 | −8.88E−16 |
| | Best | 0.00E+00 | 7.99E−07 | 0.00E+00 | 0.00E+00 | 0.00E+00 | 4.48E+01 | 0.00E+00 | 0.00E+00 | −8.88E−16 |
| | Std | 0.00E+00 | 4.00E−05 | 0.00E+00 | 0.00E+00 | 0.00E+00 | 4.92E−01 | 0.00E+00 | 0.00E+00 | 0.00E+00 |
| Fn | | F24 | F26 | F31 | F32 | F33 | F34 | F35 | F36 | |
| QLGCTSA [44] | Mean | 0.00E+00 | 3.11E−09 | 1.33E+00 | 3.72E−04 | −3.86E+00 | −1.02E+01 | −1.04E+01 | −1.05E+01 | |
| | Best | 0.00E+00 | 7.05E−10 | 9.98E−01 | 3.07E−04 | −3.86E+00 | −1.02E+01 | −1.04E+01 | −1.05E+01 | |
| | Std | 0.00E+00 | 1.53E−09 | 7.78E−01 | 2.36E−04 | 6.83E−14 | 1.36E−12 | 1.23E−12 | 6.51E−13 | |
| TSA-LEO [43] | Mean | 5.05E+03 | | | | | | | | |
| | Best | | | | | | | | | |
| | Std | 6.32E+03 | | | | | | | | |
| TL TSA | Mean | 0.00E+00 | 9.14E−01 | 1.06E+00 | 5.08E−04 | −3.86E+00 | −8.80E+00 | −1.00E+01 | −8.88E+00 | |
| | Best | 0.00E+00 | 6.08E−01 | 9.98E−01 | 3.35E−04 | −3.86E+00 | −1.02E+01 | −1.04E+01 | −1.05E+01 | |
| | Std | 0.00E+00 | 1.88E−01 | 2.52E−01 | 1.29E−04 | 2.32E−15 | 2.28E+00 | 1.35E+00 | 3.10E+00 | |

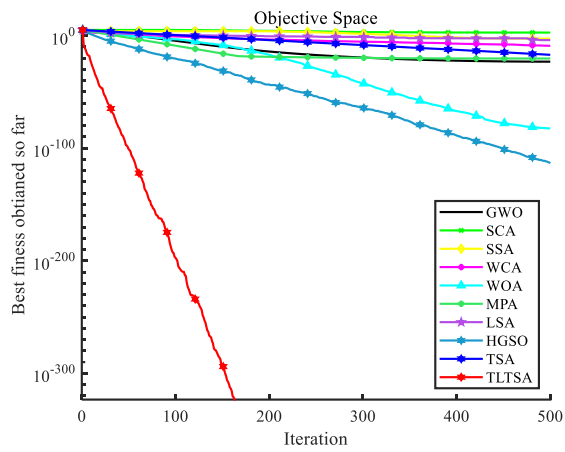
4.4.2. Convergence Curve and Boxplot Analysis

The convergence curve intuitively reflects the convergence speed and calculation precision. The boxplot is frequently used in the analysis of variance (ANOVA) test, which is useful for observing outliers and comparing algorithm stability. Figure 4 shows the convergence curves and boxplot of some benchmark functions. For F1, F3, F4, F7, F8, F10, F12-F15, F17, F19, F20, F23, F27, and F29, the TL TSA generally converged to 0 after 150–300 iterations. Its convergence curves show that it found global optimal solutions with fewer iterations. For F11, the TL TSA greatly improved convergence speed without changing the TSA calculation precision, which put its convergence speed at the forefront of all algorithms. For F2, F18, F21, and F28, where the Tent-Lévy flight strategy was introduced, the exploration and exploitation capabilities of the TL TSA were boosted greatly. For F30, some of the other algorithms had an ad-vantage in global optimization ability, but the TL TSA overcame the problem of local optimal solutions, avoided search stagnation, and improved both calculation precision and convergence speed allowing it to escape the local optimal solution. In addition, the boxplots also reflected its superior stability. It was obvious that the TL TSA box-plots had fewer or no outliers compared to the original TSA.

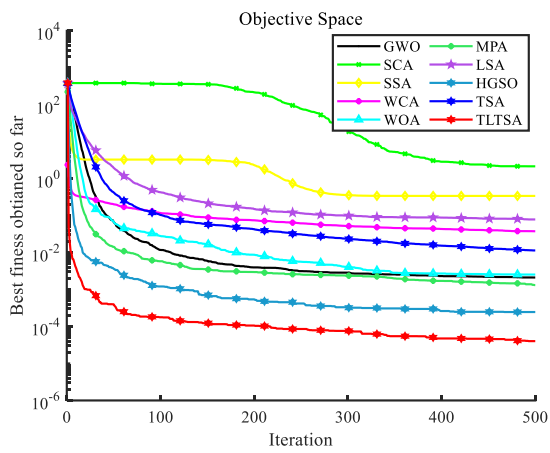
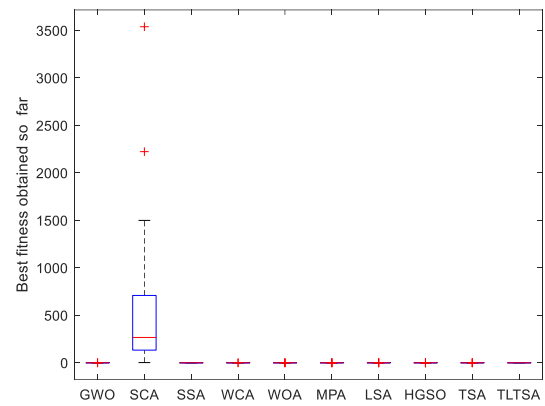
In conclusion, the proposed TL TSA combined the merits of the Lévy flight strategy and Tent map and solved the original algorithm's lack of global exploration and exploitation ability. The Tent map made step sizes of the Lévy flight strategy mutate randomly, which led to each search agent having a chance to be selected. The large step sizes of the Tent-Lévy flight strategy boosted the global exploration ability, and the small step-sized random walk improved exploitation ability such that the TL TSA maintained a dynamic equilibrium between exploration and exploitation, which not only widened the search scope to avoid the search stagnation but also enhanced the search diversity near the candidate solution. Synthesizing the above analytical results and experimental data, the calculation precision and convergence speed of the TL TSA were evidently the best. Moreover, the boxplots also attested to its strong stability and robustness. Hence, it is feasible to introduce the Tent-Lévy flight strategy into the TSA to solve the function optimization problem.

4.4.3. Statistical Test

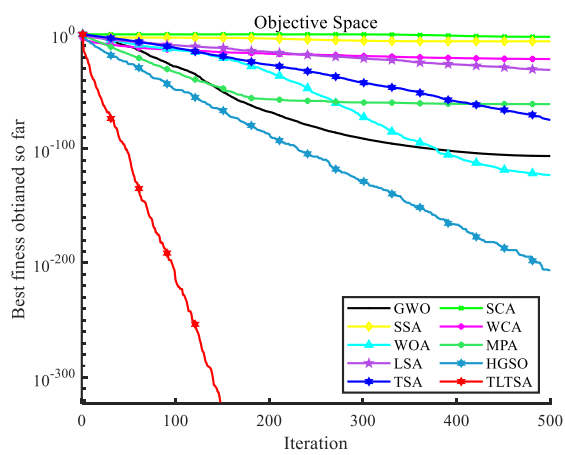
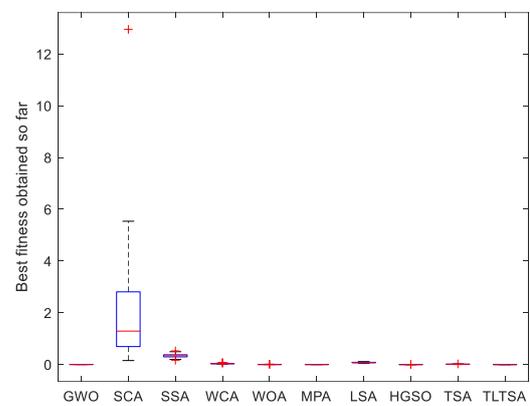
The statistical test is an important criterion for evaluating the fairness and accuracy of the proposed algorithm. A Wilcoxon nonparametric test was performed at a significance level of 0.05 to verify that the experimental results of the TL TSA were significantly different from those of other algorithms. A p -value lower than 0.05, would be sufficient proof of the null hypothesis. The test in 50 dimensions is shown in Table 10, and $p > 0.05$ is displayed in bold. NaN suggested that the result generated by the sum-of-values test was not a number. The last row shows all counts in (+/≈/−) format, where “+” means that the proposed TL TSA was superior at the 95% significance level ($\alpha = 0.05$); “−” means that the TL TSA optimization was less effective; and “≈” means that there was no significant statistical difference between the TL TSA and other algorithms. Table 12 shows the Wilcoxon test results and it is easy to see that the vast majority of p -values were less than 0.05 compared to the other algorithms. It also shows that the TL TSA had a statistically significant advantage on optimizing problems compared to other algorithms.



F1



F2



F3

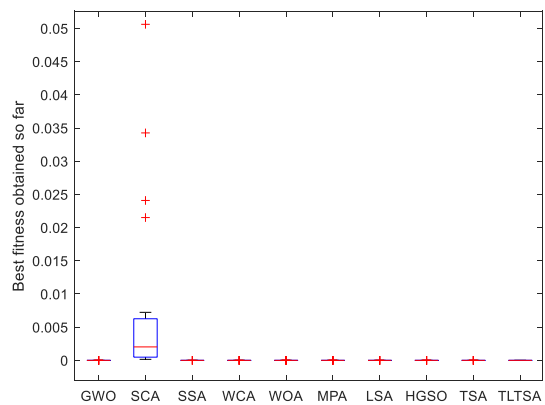
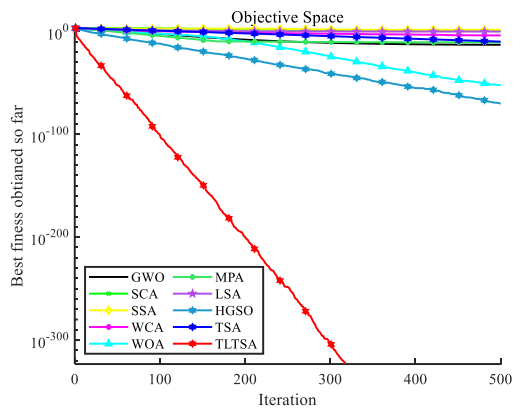
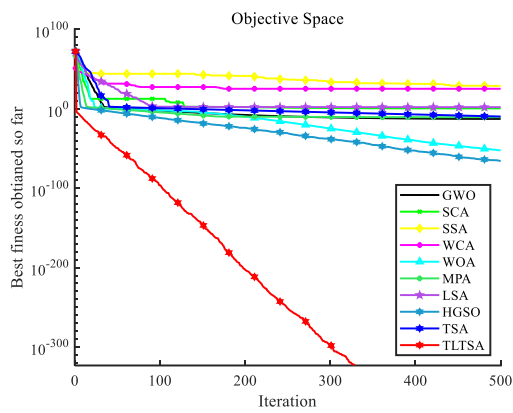
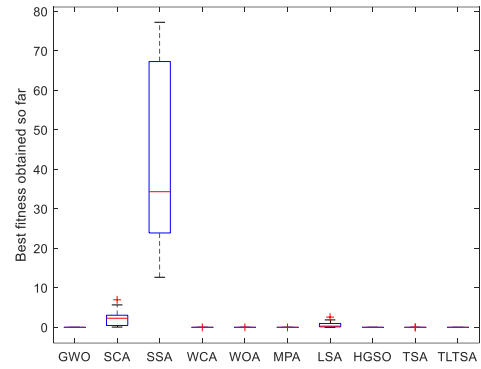


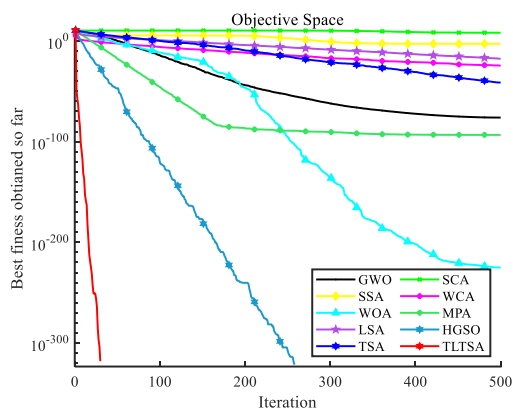
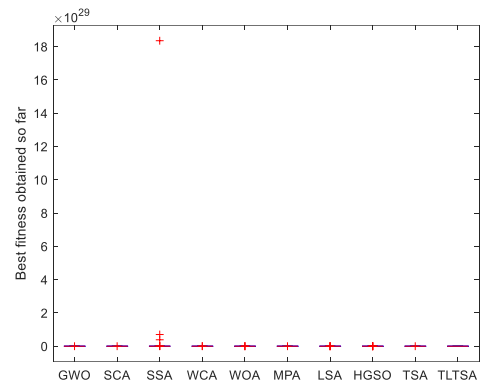
Figure 4. Cont.



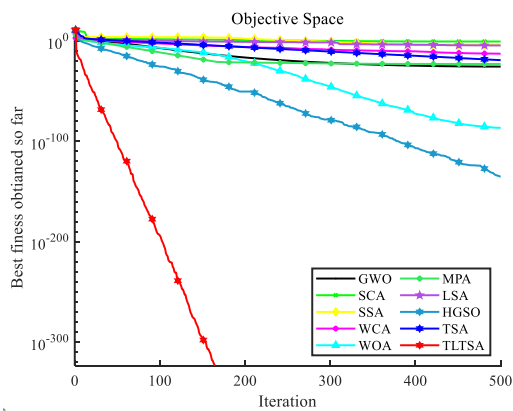
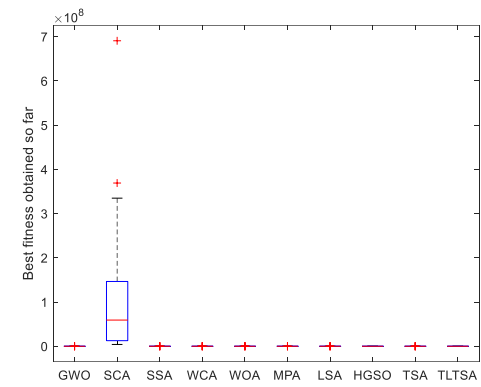
F4



F7



F8



F10

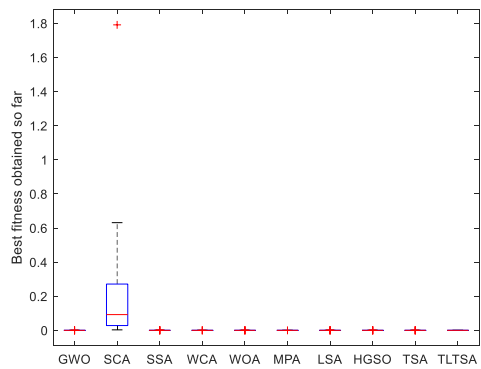


Figure 4. Cont.

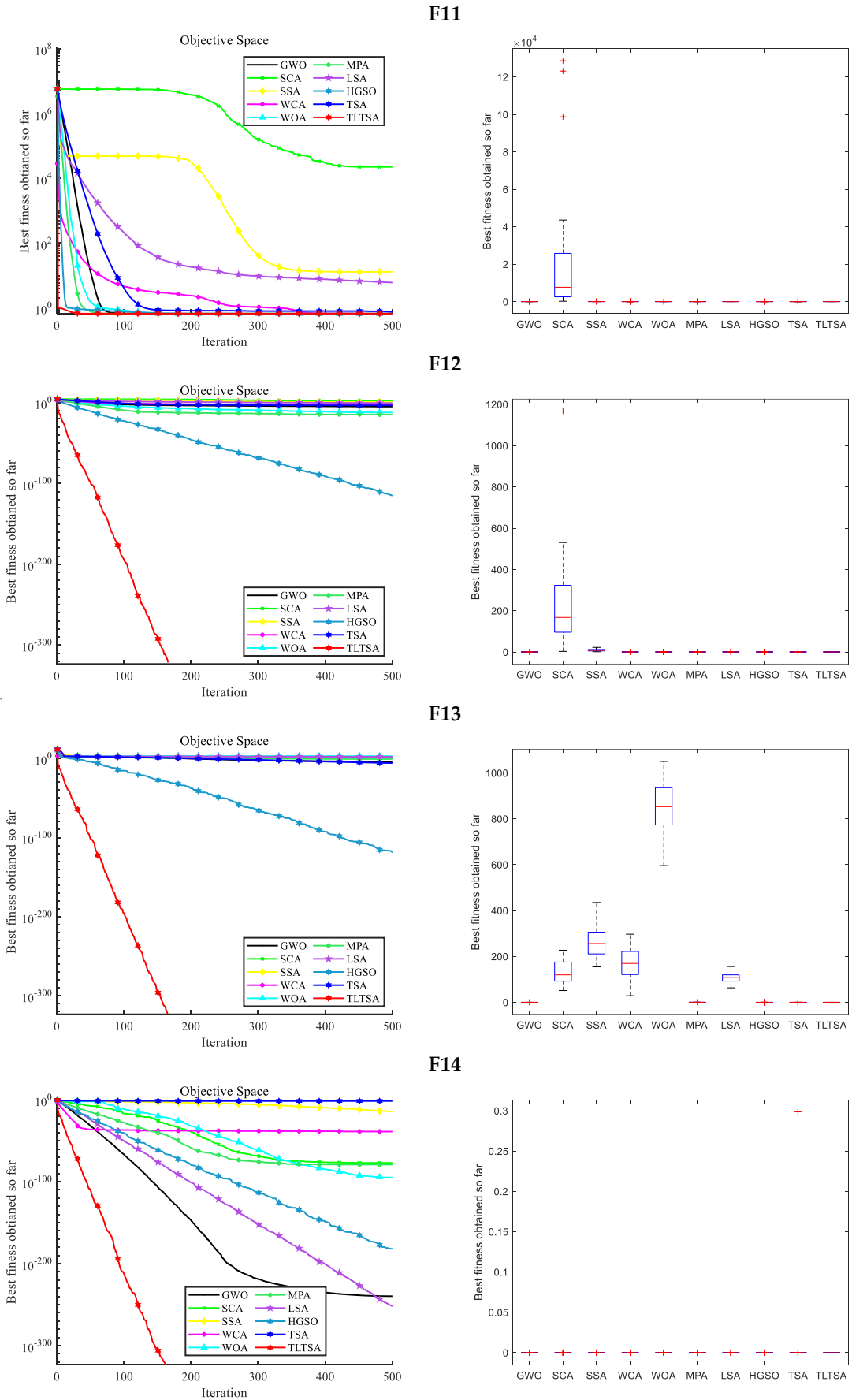
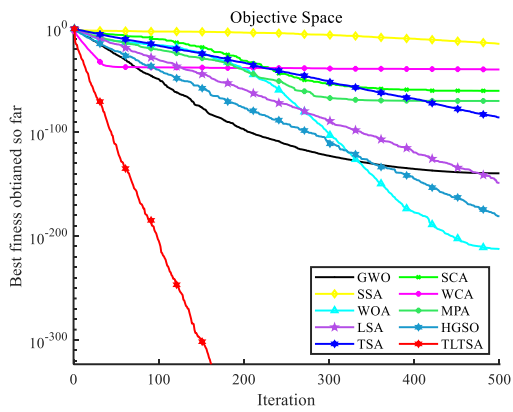
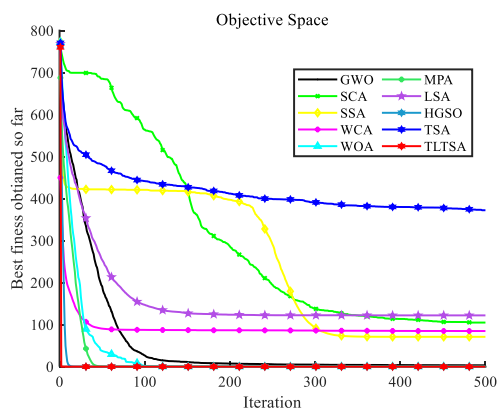
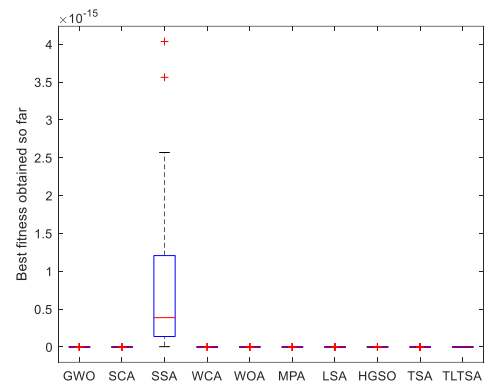


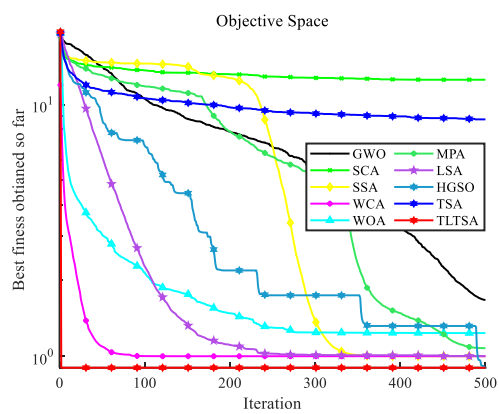
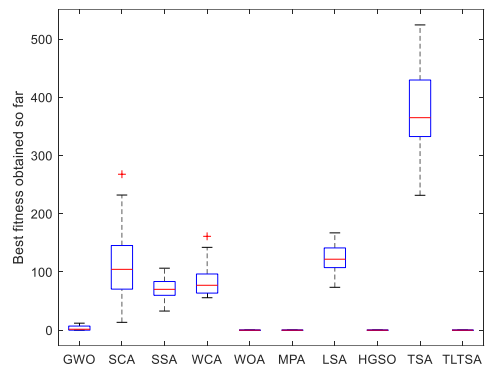
Figure 4. Cont.



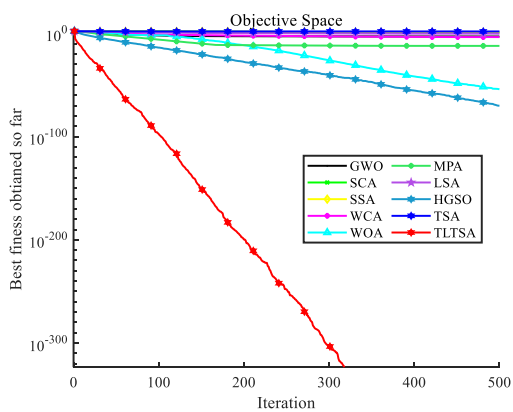
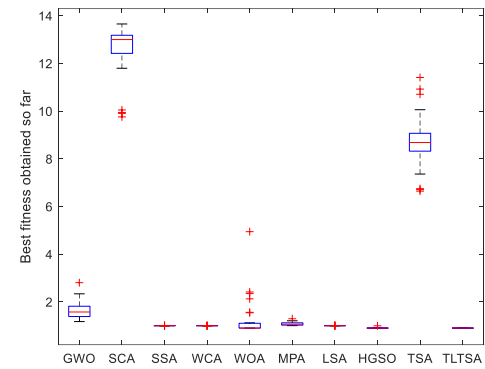
F15



F17



F18



F19

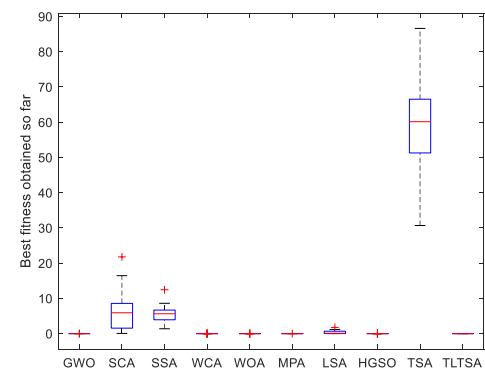


Figure 4. Cont.

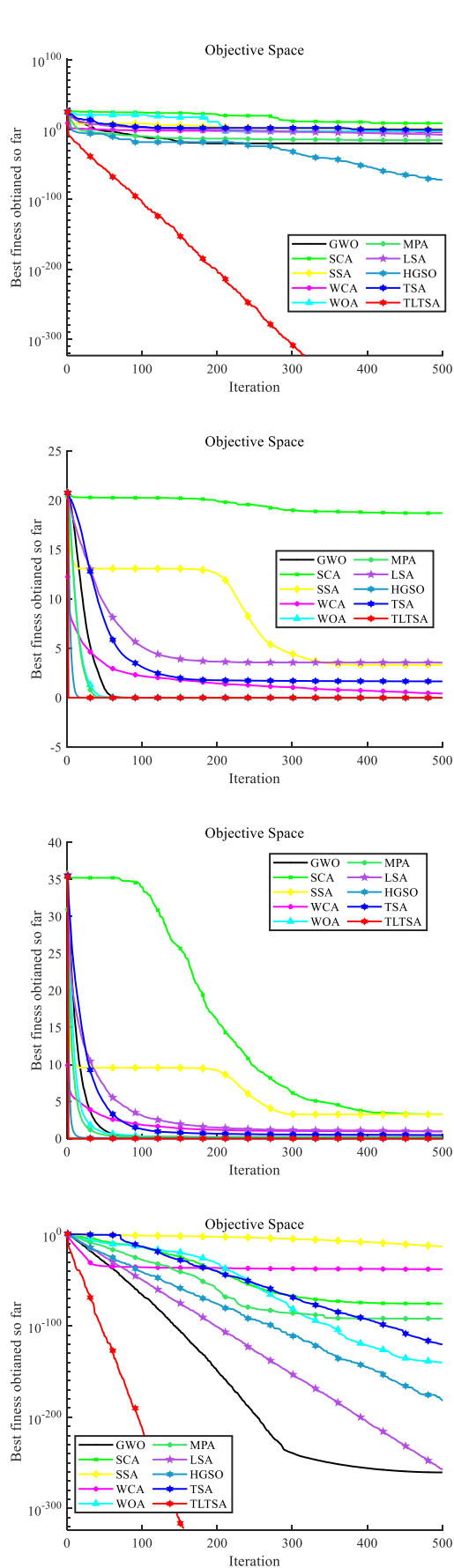
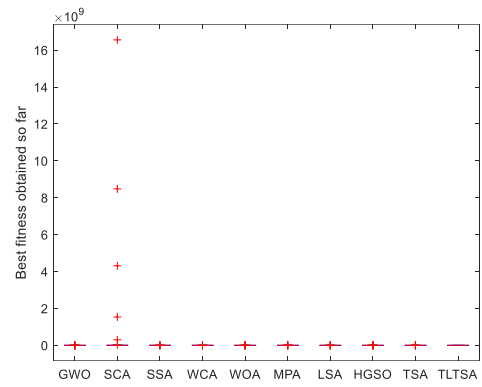
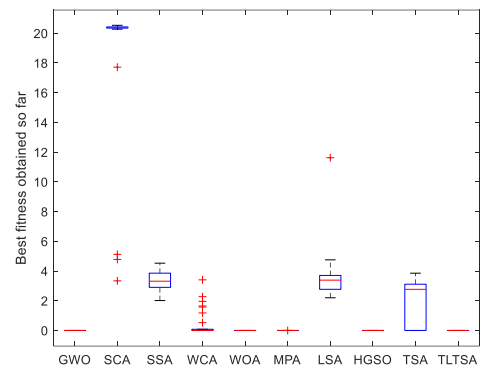


Figure 4. Cont.

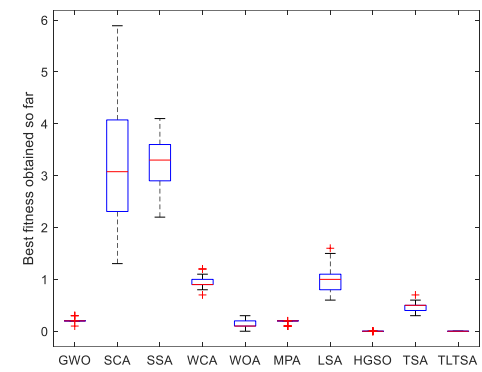
F20



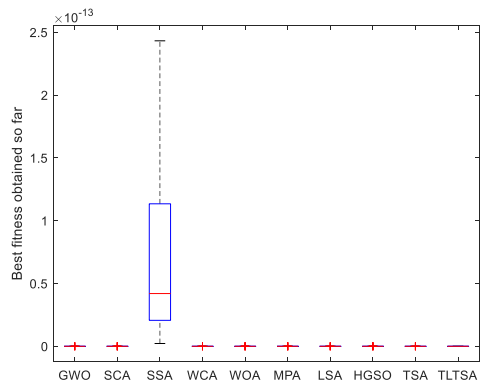
F21



F23



F27



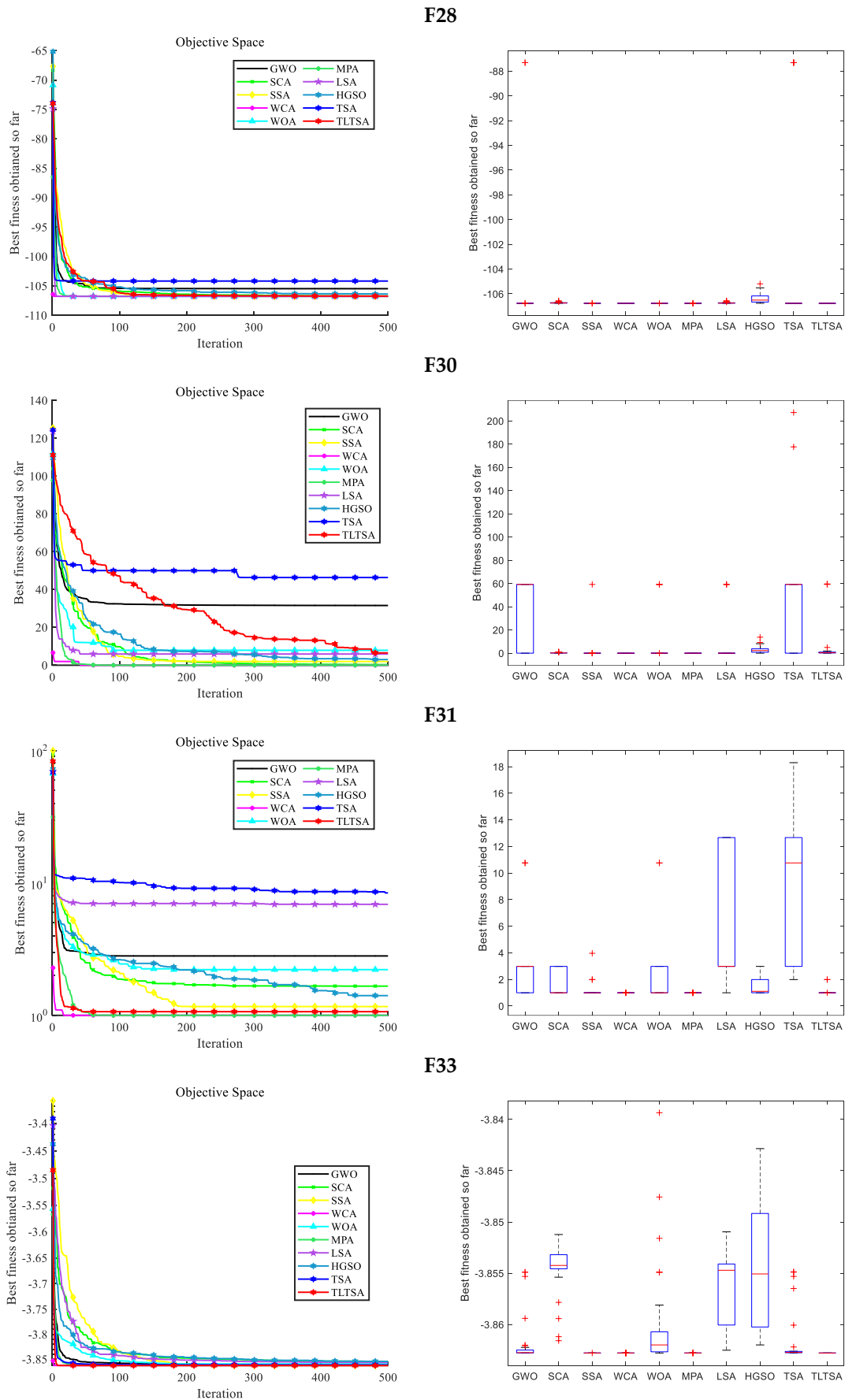
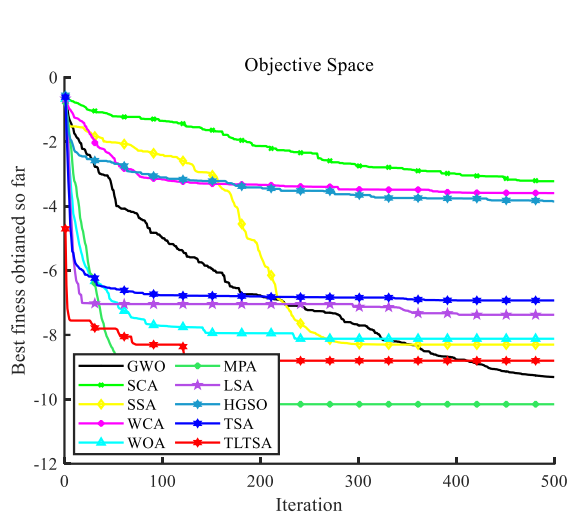
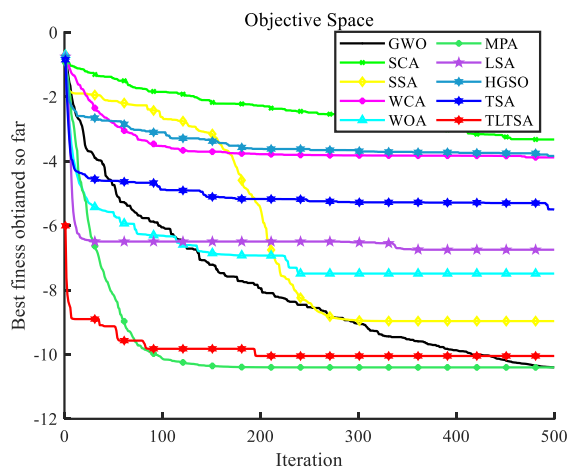
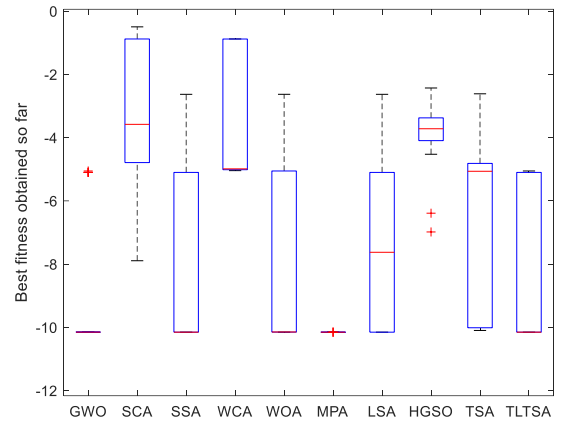


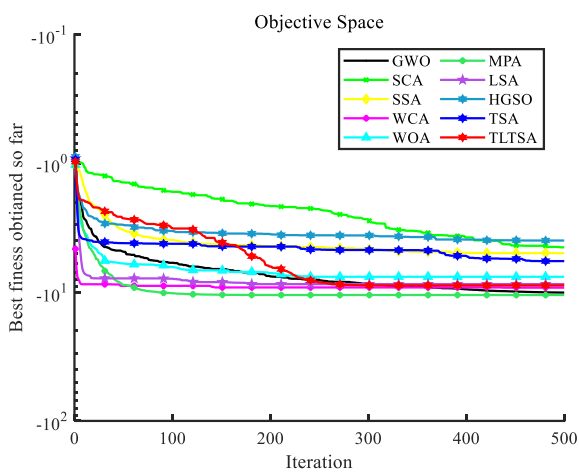
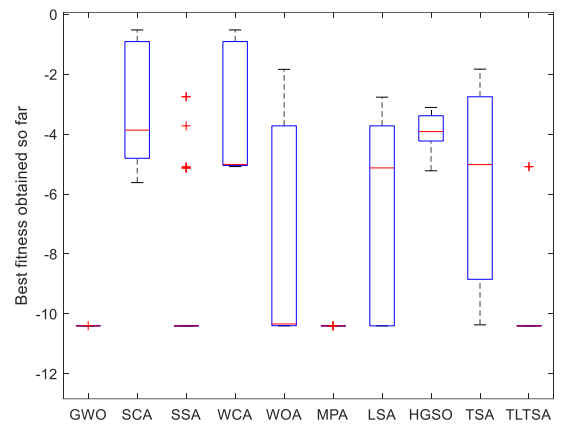
Figure 4. Cont.



F34



F35



F36

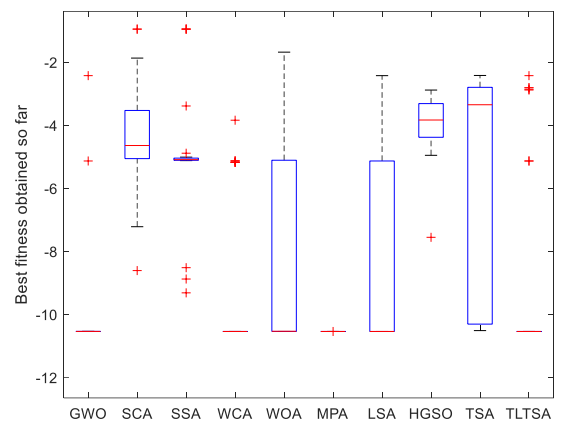


Figure 4. The convergence curve and boxplot of 36 benchmark function.

Table 12. Statistical results of the Wilcoxon rank-sum test.

| Fn | GWO | SCA | SSA | WCA | WOA | MPA | LSA | HGSO | TSA |
|-----------|----------|----------|------------------|------------------|------------------|----------|-----------------|------------------|------------------|
| F1 | 4.11E−12 | 4.11E−12 | 4.11E−12 | 4.11E−12 | 4.11E−12 | 4.11E−12 | 4.11E−12 | 4.11E−12 | 4.11E−12 |
| F2 | 7.39E−11 | 3.02E−11 | 3.02E−11 | 3.02E−11 | 1.96E−10 | 2.37E−10 | 3.02E−11 | 9.83E−08 | 3.02E−11 |
| F3 | 1.21E−12 | 1.21E−12 | 1.21E−12 | 1.21E−12 | 1.21E−12 | 1.21E−12 | 1.21E−12 | 1.21E−12 | 1.21E−12 |
| F4 | 3.02E−11 | 3.02E−11 | 3.02E−11 | 3.02E−11 | 3.02E−11 | 3.02E−11 | 3.02E−11 | 3.02E−11 | 3.02E−11 |
| F5 | 3.02E−11 | 3.02E−11 | 3.02E−11 | 3.02E−11 | 3.02E−11 | 3.02E−11 | 3.02E−11 | 3.02E−11 | 3.02E−11 |
| F6 | 3.02E−11 | 3.02E−11 | 3.02E−11 | 3.02E−11 | 3.02E−11 | 3.02E−11 | 3.02E−11 | 3.02E−11 | 3.02E−11 |
| F7 | 3.02E−11 | 3.02E−11 | 3.02E−11 | 3.02E−11 | 3.02E−11 | 3.02E−11 | 3.02E−11 | 3.02E−11 | 3.02E−11 |
| F8 | 1.21E−12 | 1.21E−12 | 1.21E−12 | 1.21E−12 | 1.21E−12 | 1.21E−12 | 1.21E−12 | NaN | 1.21E−12 |
| F9 | 4.50E−11 | 3.02E−11 | 3.02E−11 | 0.589451 | 3.02E−11 | 3.02E−11 | 5.57E−10 | 3.02E−11 | 4.50E−11 |
| F10 | 1.21E−12 | 1.21E−12 | 1.21E−12 | 1.21E−12 | 1.21E−12 | 1.21E−12 | 1.21E−12 | 1.21E−12 | 1.21E−12 |
| F11 | 3.02E−11 | 3.02E−11 | 3.02E−11 | 0.0962628 | 3.02E−11 | 3.08E−08 | 3.02E−11 | 7.09E−08 | 7.37E−10 |
| F12 | 1.10E−11 | 1.10E−11 | 1.10E−11 | 1.10E−11 | 1.10E−11 | 1.10E−11 | 1.10E−11 | 1.10E−11 | 1.10E−11 |
| F13 | 3.02E−11 | 3.02E−11 | 3.02E−11 | 3.02E−11 | 3.02E−11 | 3.02E−11 | 3.02E−11 | 3.02E−11 | 3.02E−11 |
| F14 | 1.21E−12 | 1.21E−12 | 1.21E−12 | 1.21E−12 | 1.21E−12 | 1.21E−12 | 1.21E−12 | 1.21E−12 | 1.21E−12 |
| F15 | 1.21E−12 | 1.21E−12 | 1.21E−12 | 1.21E−12 | 1.21E−12 | 1.21E−12 | 1.21E−12 | 1.21E−12 | 1.21E−12 |
| F16 | 3.02E−11 | 3.02E−11 | 1.85E−03 | 1.48E−11 | 2.00E−06 | 1.83E−11 | 1.99E−11 | 2.20E−07 | 6.52E−09 |
| F17 | 4.50E−12 | 1.21E−12 | 1.21E−12 | 1.21E−12 | 0.333711 | NaN | 1.21E−12 | NaN | 1.21E−12 |
| F18 | 1.21E−12 | 1.21E−12 | 1.21E−12 | 1.21E−12 | 1.26E−05 | 1.21E−12 | 1.21E−12 | 0.333711 | 1.21E−12 |
| F19 | 3.02E−11 | 3.02E−11 | 3.02E−11 | 3.02E−11 | 3.02E−11 | 3.02E−11 | 3.02E−11 | 3.02E−11 | 3.02E−11 |
| F20 | 1.27E−11 | 1.27E−11 | 1.27E−11 | 1.27E−11 | 1.27E−11 | 1.27E−11 | 1.27E−11 | 1.27E−11 | 1.27E−11 |
| F21 | 8.85E−12 | 8.85E−12 | 8.85E−12 | 8.85E−12 | 3.53E−06 | 8.85E−12 | 8.85E−12 | 2.70E−03 | 8.85E−12 |
| F22 | 3.02E−11 | 3.02E−11 | 3.02E−11 | 8.15E−11 | 4.64E−05 | 3.02E−11 | 0.118817 | 2.57E−07 | 3.34E−11 |
| F23 | 3.02E−11 | 3.02E−11 | 3.02E−11 | 2.46E−11 | 2.35E−10 | 4.11E−11 | 3.02E−11 | 1.68E−04 | 3.02E−11 |
| F24 | 2.79E−03 | 1.21E−12 | 1.21E−12 | 1.21E−12 | 0.160802 | NaN | 1.21E−12 | NaN | 6.61E−05 |
| F25 | 3.02E−11 | 3.02E−11 | 3.02E−11 | 3.02E−11 | 3.02E−11 | 3.02E−11 | 3.02E−11 | 8.99E−11 | 3.56E−04 |
| F26 | 3.02E−11 | 3.02E−11 | 3.02E−11 | 3.02E−11 | 3.02E−11 | 3.02E−11 | 1.29E−06 | 5.26E−04 | 3.02E−11 |
| F27 | 1.21E−12 | 1.21E−12 | 1.21E−12 | 1.21E−12 | 1.21E−12 | 1.21E−12 | 1.21E−12 | 1.21E−12 | 1.21E−12 |
| F28 | 5.57E−10 | 3.01E−11 | 4.43E−03 | 1.29E−11 | 3.02E−11 | 2.83E−11 | 1.46E−11 | 3.20E−09 | 2.50E−03 |
| F29 | 3.03E−03 | 3.02E−11 | 0.0594279 | 1.69E−11 | 0.311188 | 2.33E−11 | 1.88E−11 | 3.02E−11 | 2.05E−03 |
| F30 | 6.77E−05 | 8.46E−09 | 0.56922 | 1.21E−12 | 6.77E−05 | 2.10E−11 | 2.47E−08 | 1.25E−05 | 1.95E−03 |
| F31 | 2.68E−10 | 1.78E−07 | 4.84E−10 | 0.198282 | 3.27E−10 | 2.18E−07 | 8.02E−12 | 8.67E−10 | 1.69E−11 |
| F32 | 1.77E−03 | 7.04E−07 | 2.39E−08 | 5.43E−10 | 2.71E−02 | 3.02E−11 | 2.15E−02 | 0.0701266 | 0.0750587 |
| F33 | 8.10E−10 | 3.02E−11 | 0.0656713 | 4.08E−12 | 0.0678689 | 7.57E−12 | 1.72E−12 | 0.17145 | 3.02E−11 |
| F34 | 9.70E−04 | 7.21E−05 | 1.30E−10 | 1.30E−10 | 3.04E−04 | 7.51E−03 | 0.228715 | 5.36E−11 | 3.49E−06 |
| F35 | 5.35E−07 | 1.07E−07 | 2.36E−10 | 3.21E−11 | 9.76E−09 | 7.30E−07 | 0.202628 | 1.41E−11 | 4.77E−09 |
| F36 | 3.50E−03 | 9.79E−05 | 4.22E−04 | 1.67E−06 | 4.46E−04 | 4.71E−04 | 1.22E−02 | 6.77E−05 | 4.35E−05 |
| + / ≈ / − | 36/0/0 | 36/0/0 | 33/0/3 | 33/0/3 | 32/0/4 | 34/2/0 | 33/0/3 | 30/3/3 | 35/0/1 |

5. TL TSA for Complex Problems in the Engineering Field

An improved optimization algorithm was proposed to settle practical problems in engineering more efficiently. The benchmark functions were different because engineering problems are often constrained. In addition, the optimal solutions to most engineering problems are not clear. Therefore, a practical, constrained engineering problem is an important criterion for measuring the performance of optimization algorithms. In this section, three constrained engineering problems were selected to verify the ability of the TL TSA to solve them: Three-bar truss design problem, welded beam design problem, and optimal design of an industrial refrigeration system. The best results of each experiment are highlighted in bold.

5.1. Three-Bar Truss Design Problem

The three-bar truss design problem is a classic in the engineering structure field. The optimization goal is to design a truss with the smallest weight while satisfying three constraints on stress, deflection, and buckling. The structural model and parameters are displayed in Figure 5. The mathematical expression is defined as follows [67]:

Deem:

$$\vec{x} = [x_1, x_2] = [A_1, A_2] \tag{27}$$

Objective function:

$$f(\vec{x}) = (2\sqrt{2}x_1 + x_2) \times L \tag{28}$$

Constraint functions:

$$g_1(\vec{x}) = \frac{\sqrt{2}x_1 + x_2}{\sqrt{2}x_1^2 + 2x_1x_2} P - \sigma \leq 0$$

$$g_2(\vec{x}) = \frac{x_2}{\sqrt{2}x_1^2 + 2x_1x_2} P - \sigma \leq 0 \tag{29}$$

$$g_3(\vec{x}) = \frac{1}{\sqrt{2}x_2 + x_1} P - \sigma \leq 0$$

Variable range:

$$0 \leq x_1, x_2 \leq 1$$

where $L = 100 \text{ cm}$, $P = 2 \frac{\text{KN}}{\text{cm}^2}$, $\sigma = 2 \frac{\text{KN}}{\text{cm}^2}$.

Table 13 shows the experimental results of the TL TSA and other algorithms. According to the experimental results and convergence curve in Figure 6, the results for the TL TSA were the same as those for the MPA, WCA, and SSA; its optimal cost was the smallest. This demonstrated that the proposed TL TSA is feasible for settling the three-bar truss design problem.

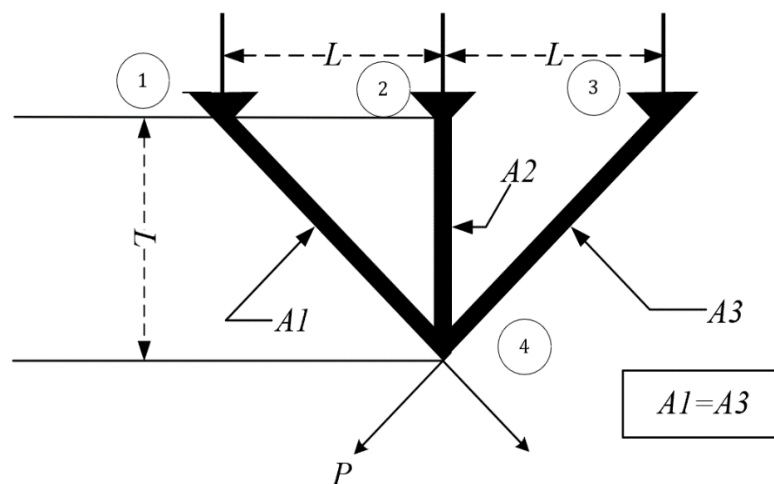


Figure 5. Three-bar truss design problem.

Table 13. Comparison of TL TSA with other optimization algorithms for three-bar truss design problem.

| Algorithm | Optimal Variable A_1 | Optimal Variable A_2 | Optimal Cost |
|-----------|------------------------|------------------------|-----------------|
| GWO | 0.78693 | 0.28779 | 186.3860 |
| SCA | 0.77940 | 0.30414 | 186.4062 |
| SSA | 0.78685 | 0.28801 | 186.3859 |
| WCA | 0.78685 | 0.28801 | 186.3859 |
| WOA | 0.83937 | 0.19509 | 186.7164 |
| MPA | 0.78685 | 0.28801 | 186.3859 |
| LSA | 0.79784 | 0.26626 | 186.4503 |
| HGSO | 0.78921 | 0.28358 | 186.4424 |
| TSA | 0.78698 | 0.28764 | 186.3864 |
| TL TSA | 0.78685 | 0.28801 | 186.3859 |

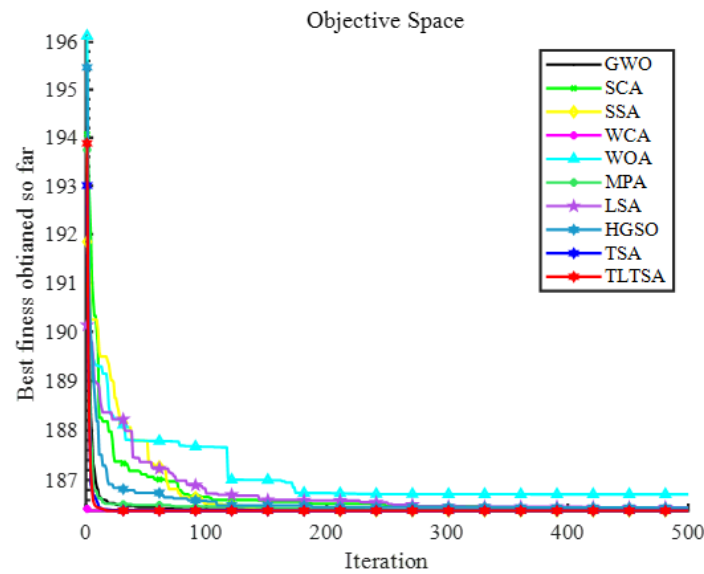


Figure 6. Convergence curve for three-bar truss design problem.

5.2. Welded Beam Design Problem

The welded beam design problem is also well-known. The optimization objective was found to be the most suitable value for each variable in calculating the minimum cost of a welded beam subject to shear stress (τ), beam-bending stress (σ), bar buckling load (P_c) and beam end deflection (δ). This design problem is influenced by four variables: weld thickness (h), clamped-bar length (l), bar height (t), and bar thickness (b). The structural model and the meaning of the parameters are shown in Figure 7. The mathematical expression is listed below [68]:

Deem:

$$\vec{z} = [z_1, z_2, z_3, z_4] = [h, l, t, b] \tag{30}$$

Objective function:

$$f(\vec{z}) = 1.10471z_1^2z_2 + 0.04811z_3z_4(14 + z_2) \tag{31}$$

Constraint functions:

$$\begin{aligned} g_1(\vec{z}) &= \tau(\vec{z}) - 13600 \leq 0 \\ g_2(\vec{z}) &= \sigma(\vec{z}) - 30000 \leq 0 \\ g_3(\vec{z}) &= \delta(\vec{z}) - 0.25 \leq 0 \\ g_4(\vec{z}) &= z_1 - z_4 \leq 0 \\ g_5(\vec{z}) &= 6000 - P_c(\vec{z}) \leq 0 \\ g_6(\vec{z}) &= 0.125 - z_1 \leq 0 \\ g_7(\vec{z}) &= 1.10471z_1^2z_2 + 0.04811z_3z_4(14 + z_2) - 5 \leq 0 \end{aligned} \tag{32}$$

Variable range:

$$0.1 \leq z_1, z_2 \leq 2, 0.1 \leq z_3, z_4 \leq 10$$

Other parameters:

$$\begin{aligned} \tau(\vec{z}) &= \sqrt{(\tau')^2 + (z_2 \tau' \tau'') / \sqrt{\frac{(z_2^2 + (z_1 + z_3)^2)}{4}} + (\tau'')^2} \\ \tau' &= \frac{6000}{\sqrt{2}z_1z_2}, \sigma(\vec{z}) = \frac{504,000}{z_3^2z_4}, \delta(\vec{z}) = \frac{65,856,000}{(30 \times 10^6)z_1z_3^3} \\ \tau'' &= \frac{6000(14 + 0.5z_2)\sqrt{0.25(z_2^2 + (z_1 + z_3)^2)}}{2 \left[0.707z_1z_2 \left(\frac{1}{12z_2^2} + 0.25(z_1 + z_3)^2 \right) \right]} \end{aligned} \tag{33}$$

Table 14 shows the comparison between the proposed TL TSA and the other algorithms in optimal variables and optimal costs. The Figure 8 displays the convergence curves. It can be seen that the proposed TL TSA is the most competitive. TL TSA gains the optimal cost $f(z_{1-4}) = 1.6952$ at the most suitable position $(z_1, z_2, z_3, z_4) = (0.20573, 3.2530, 9.0336, 0.20573)$, and ranked first. The experimental results showed that it had strong global exploration and exploitation ability to optimize the welded beam design problem to reduce engineering costs.

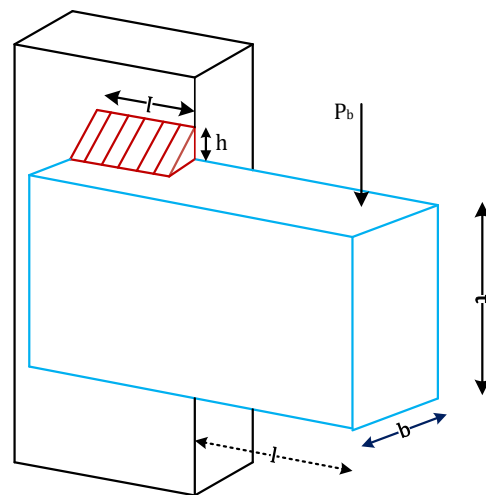


Figure 7. Welded beam design problem.

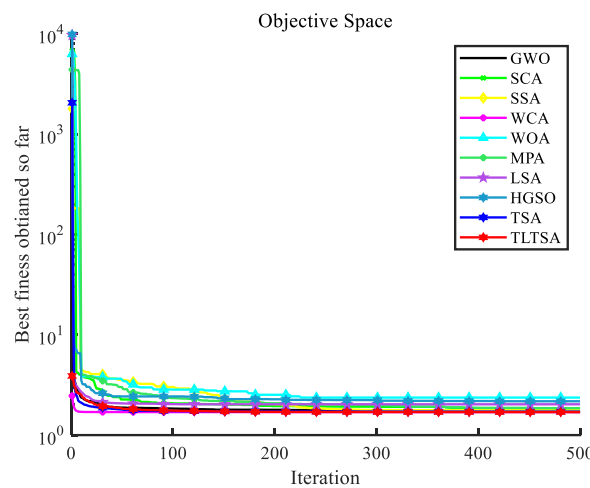


Figure 8. Convergence curve for welded design problem.

Table 14. Comparison of TL TSA with other optimization algorithms for welded beam design problem.

| Algorithm | Optimal Variable | | | | Optimal Cost |
|---------------|------------------|---------------|---------------|----------------|---------------|
| | h | l | t | b | |
| GWO | 0.20095 | 3.3454 | 9.0465 | 0.20569 | 1.7000 |
| SCA | 0.20044 | 3.8852 | 9.4553 | 0.20645 | 1.8402 |
| SSA | 0.20648 | 3.2282 | 9.0796 | 0.20645 | 1.7686 |
| WOA | 0.21850 | 4.1900 | 5.6288 | 0.53853 | 2.3655 |
| MPA | 0.16971 | 3.9050 | 10 | 0.20207 | 1.8539 |
| LSA | 0.20573 | 3.2530 | 9.0366 | 0.20573 | 2.0274 |
| HGSO | 0.14780 | 4.8333 | 8.9045 | 0.21856 | 2.1737 |
| TSA | 0.20054 | 3.4016 | 9.0598 | 0.20624 | 1.7142 |
| TL TSA | 0.20573 | 3.2530 | 9.0366 | 0.20573 | 1.6952 |

5.3. Optimal Design Problem of Industrial Refrigeration System

As a nonlinear inequality-constrained optimization design problem, because it contains a lot of constraints, the optimal design problem of the industrial refrigeration system is suitable for evaluating the ability of the algorithm to solve an actual engineering problem. The optimal objective is to reduce the design costs as much as possible. The mathematical model is [69]:

Objective function:

$$\begin{aligned}
 f(\vec{x}) = & 63098.88x_2x_4x_{12} + 5441.5x_2^2x_{12} + 115055.5x_2^{1.664}x_6 + 6172.27x_2^2x_6 \\
 & + 63098.88x_1x_3x_{11} + 5441.5x_1^2x_{11} + 115055.5x_1^{1.664}x_5 + 6172.27x_1^2x_5 \\
 & + 140.53x_1x_{11} + 281.29x_3x_{11} + 70.26x_1^2 + 281.29x_1x_3 \\
 & + 281.29x_3^2 + 14437x_8^{1.8812}x_{12}^{0.3424}x_{10}x_{14}^{-1}x_1^2x_7x_9^{-1} \\
 & + 20470.2x_7^{2.893}x_{11}^{0.316}x_1^2
 \end{aligned} \tag{34}$$

Constraint functions:

$$\begin{aligned}
 g_1(\vec{x}) &= 1.524x_7^{-1} \leq 1 \\
 g_2(\vec{x}) &= 1.524x_8^{-1} \leq 1 \\
 g_3(\vec{x}) &= 0.07789x_1 - 2x_7^{-1}x_9 - 1 \leq 0 \\
 g_4(\vec{x}) &= 7.05305x_9^{-1}x_1^2x_{10}x_8^{-1}x_2^{-1}x_{14}^{-1} - 1 \leq 0 \\
 g_5(\vec{x}) &= 0.0833x_{13}^{-1}x_{14} - 1 \leq 0 \\
 g_6(\vec{x}) &= 47.136x_2^{0.333}x_{10}^{-1}x_{12} - 1.333x_8x_{13}^{2.1195} + 62.08x_{13}^{2.1195}x_{12}^{-1}x_8^{0.2}x_{10}^{-1} - 1 \leq 0 \\
 g_7(\vec{x}) &= 0.04771x_{10}x_8^{1.8812}x_{12}^{0.3424} - 1 \leq 0 \\
 g_8(\vec{x}) &= 0.0488x_9x_7^{1.893}x_{11}^{0.316} - 1 \leq 0 \\
 g_9(\vec{x}) &= 0.099x_1x_3^{-1} - 1 \leq 0 \\
 g_{10}(\vec{x}) &= 0.0193x_2x_4^{-1} - 1 \leq 0 \\
 g_{11}(\vec{x}) &= 0.0298x_1x_5^{-1} - 1 \leq 0 \\
 g_{12}(\vec{x}) &= 0.056x_2x_6^{-1} - 1 \leq 0 \\
 g_{13}(\vec{x}) &= 2x_9^{-1} - 1 \leq 0 \\
 g_{14}(\vec{x}) &= 2x_{10}^{-1} - 1 \leq 0 \\
 g_{15}(\vec{x}) &= x_{12}x_{11}^{-1} - 1 \leq 0
 \end{aligned} \tag{35}$$

Variable range:

$$0.001 \leq x_i \leq 5, i = 1, \dots, 14$$

Six well-known meta-heuristic optimization algorithms—GWO, SSA, WCA, WOA, and HGSO, and the original TSA—were selected for comparison with TL TSA. The experimental results of optimal costs and variables are given in Table 15. The TL TSA obtained optimal costs $f(x_{1-14}) = 0.19637$, which were significantly lower. In addition, the convergence curves in Figure 9 also indicate the proposed TL TSA is superior.

Table 15. Comparison of TL TSA with other algorithms for optimal design problem of industrial refrigeration system.

| Optimal Value | GWO | SSA | WCA | WOA | HGSO | TSA | TL TSA |
|---------------------------|-----------|-----------|-----------|-----------|-----------|-----------|------------------|
| Optimal variable x_1 | 0.001 | 0.001 | 0.001 | 0.001 | 0.0010561 | 0.001 | 0.001 |
| Optimal variable x_2 | 0.0010912 | 0.001 | 0.001 | 0.001 | 0.0029744 | 0.0010534 | 0.0010461 |
| Optimal variable x_3 | 0.0010052 | 0.0010118 | 0.001 | 0.015982 | 0.0028955 | 0.0010950 | 0.0010241 |
| Optimal variable x_4 | 0.0013333 | 4.8584 | 0.001 | 0.001 | 0.0032518 | 0.0076186 | 0.10488 |
| Optimal variable x_5 | 0.0010012 | 2.7978 | 0.001 | 0.001 | 0.1921 | 0.0048673 | 0.074202 |
| Optimal variable x_6 | 0.0011156 | 1.2464 | 0.001 | 0.011293 | 0.0045721 | 0.0040403 | 0.01525 |
| Optimal variable x_7 | 1.5252 | 3.5466 | 1.5240 | 1.5787 | 2.1326 | 1.5383 | 1.7251 |
| Optimal variable x_8 | 1.5249 | 3.9266 | 1.5240 | 1.5235 | 4.4739 | 1.5280 | 1.5473 |
| Optimal variable x_9 | 5 | 3.7794 | 5 | 2.8120 | 2.1012 | 4.8173 | 4.5901 |
| Optimal variable x_{10} | 2.5139 | 2.0191 | 2 | 3.7725 | 2.0096 | 2.1429 | 2.3255 |
| Optimal variable x_{11} | 0.019292 | 0.001 | 0.001 | 0.023963 | 0.0016401 | 0.0089912 | 0.001 |
| Optimal variable x_{12} | 0.019167 | 0.001 | 0.001 | 0.001 | 0.0015673 | 0.0083106 | 0.001 |
| Optimal variable x_{13} | 0.032051 | 0.0057349 | 0.0072934 | 0.0074685 | 0.0020327 | 0.020283 | 0.0057234 |
| Optimal variable x_{14} | 0.38109 | 0.065408 | 0.087557 | 0.061517 | 0.001172 | 0.24036 | 0.049644 |
| Optimal cost | 286.4233 | 357.3893 | 93.9437 | 1.6727 | 59.7011 | 211.5825 | 0.19637 |

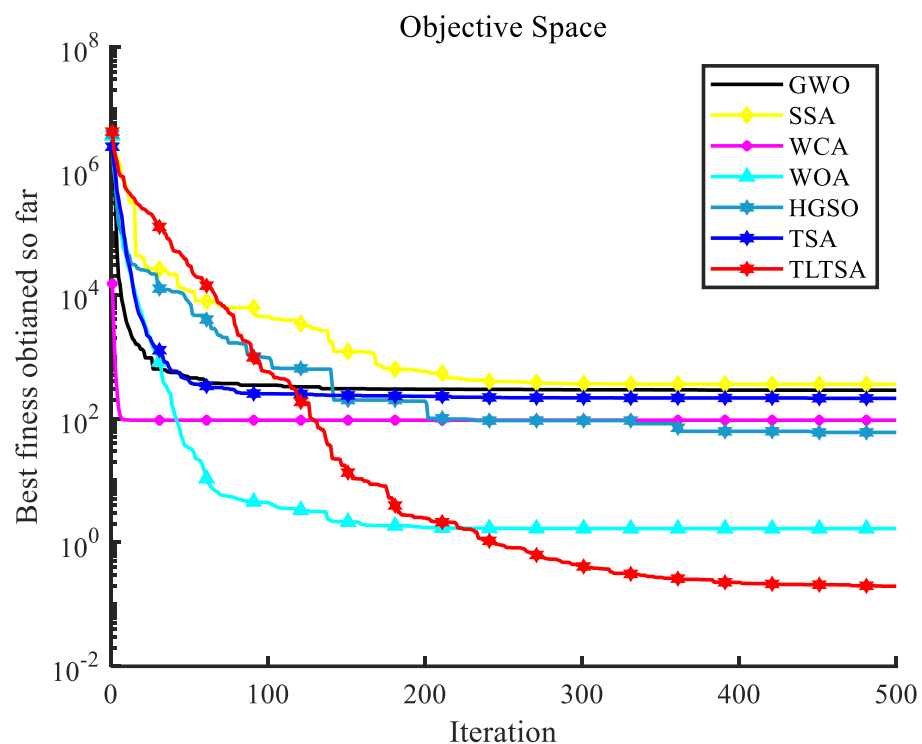


Figure 9. Convergence curve for optimal design problem of industrial refrigeration system.

6. Conclusions and Future Work

In this paper, an improved TSA based on Chaotic-Lévy flight strategy (CL TSA) was proposed to overcome defects of the original algorithm, such as premature convergence and poor solution accuracy. As a random walk strategy, Chaotic-Lévy flight made the search agents produce a mass of small step-sized moves and a small number of large ones

when converging towards the candidate solution. The small-step random walks enabled search agents to exploit the vicinity of the candidate solution fully, which improves its exploitation ability. The mutability generated by the large-step random walks gave the search agent a chance to appear at any position in the solution space, thereby boosting the global exploration capability of the CLTSA and increasing tunicate population diversity. However, it was crucial to combine a suitable chaotic map with Lévy flight, and from a comparison of chaotic maps, the tent map was the most appropriate. Because the chaotic values generated by the tent map were more evenly distributed in $(0, 1)$, the combination with the step sizes generated by the Lévy flight strategy had a high degree of randomness, so it was easier for TL TSA to strengthen the richness of the population and avoid becoming trapped in local minimization. In addition, the values in $(0,1)$ generated by the tent map ensured that the search agents moved within the search range as much as possible. The Tent-Lévy flight strategy not only helped the search agents find potential areas, but also strengthened exploration around the current solution, which made the algorithm maintain an exploration–exploitation equilibrium that enhanced the TL TSA optimization efficiency.

To verify the feasibility of the TL TSA in finding the optimal solution and solving the practical problem, 36 benchmark functions and 3 practical constrained engineering problems were selected for contrast experiments. The data indicates that the proposed TL TSA was a great improvement over the original algorithm in performing test functions. TL TSA not only overcame the shortcomings of the original algorithm, such as search stagnation and premature convergence, but also had greater calculation accuracy. Another advantage was that it had a smaller standard deviation, which meant greater stability. In addition, the convergence curves also attested to a more competitive convergence speed. In addition, the design costs optimized by the TL TSA for three engineering design problems were clearly lower than those of other algorithms. Therefore, TL TSA, the best algorithm among the CL TSAs, provides new possibilities for solving real-world engineering problems.

Even though our proposed TL TSA is a great improvement over the original TSA, it still had research value. Our research is limited to combining one-dimensional chaotic mapping with Lévy flight. In the following research, we will consider applying two-dimensional chaotic mapping to algorithm optimization. Furthermore, because of the characteristic antenna design problems, the proposed TL TSA can only optimize the antenna with continuous parameters (the antenna structure needs to be specified), and we will propose the binary and multi-objective versions of the TSA algorithm to improve the TL TSA's optimization efficiency to solve complex antenna and frequency-selective surface design problems.

Author Contributions: Conceptualization, Y.C. and J.D.; methodology, Y.C. and J.D.; software, Y.C.; validation, Y.C., R.S. and J.D.; formal analysis, R.S.; investigation, Y.C. and J.D.; resources, J.D.; data curation, R.S.; writing—original draft preparation, Y.C.; writing—review and editing, R.S. and J.D.; visualization, R.S.; supervision, J.D.; project administration, Y.C., R.S. and J.D.; funding acquisition, J.D. and R.S. All authors have read and agreed to the published version of the manuscript.

Funding: This research was funded in part by the National Natural Science Foundation of China under grant numbers 61801521 and 61971450, in part by the Natural Science Foundation of Hunan Province under grant number 2018JJ2533 and 2022JJ30052, and in part by the Fundamental Research Funds for the Central Universities under grant number 2018gczd014 and 20190038020050.

Institutional Review Board Statement: Not applicable.

Informed Consent Statement: Not applicable.

Data Availability Statement: Not applicable.

Conflicts of Interest: The authors declare no conflict of interest.

Appendix A

Table A1. Mathematical expressions of unimodal benchmark functions.

| Function Expressions |
|---|
| $F1 = \sum_{i=1}^n x_i^2$ |
| $F2 = \sum_{i=1}^n ix_i^4 + random[0, 1]$ |
| $F3 = \sum_{i=1}^D x_i ^{i+1}$ |
| $F4 = \sum_{i=1}^n x_i $ |
| $F5 = max(x_i , 1 \leq i \leq n)$ |
| $F6 = \sum_{i=1}^n \left(\sum_{j=1}^i x_j\right)^2$ |
| $F7 = \sum_{i=1}^n x_i + \prod_{i=1}^n x_i $ |
| $F8 = \sum_{i=1}^n x_i^{10}$ |
| $F9 = \sum_{i=1}^{n-1} [100(x_{i+1} - x_i^2)^2 + (x_i - 1)^2]$ |
| $F10 = \sum_{i=1}^{n-1} (x_i^2)^{(x_{i+1}^2+1)} + (x_{i+1}^2)^{(x^2+1)}$ |
| $F11 = (x_1 - 1)^2 + \sum_{i=2}^D i(2x_i^2 - x_{i-1})^2$ |
| $F12 = \sum_{i=1}^{\frac{D}{4}} (x_{4i-3} + 10x_{4i-2})^2 + 5(x_{4i-1} - 10x_{4i})^2 + (x_{4i-2} - x_{4i-1})^2 + 10(x_{4i-3} - x_{4i})^2$ |
| $F13 = \sum_{i=1}^n x_i^2 + \left(\sum_{i=1}^n 0.5ix_i\right)^2 + \left(\sum_{i=1}^n 0.5ix_i\right)^4$ |
| $F14 = 2x_1^2 - 1.05x_1^4 + \frac{x_1^6}{6} + x_1x_2 + x_2^2$ |
| $F15 = 0.26(x_1^2 + x_2^2) - 0.48x_1x_2$ |
| $F16 = 100(x_2 - x_1^2)^2 + (1 - x_1)^2$ |

Table A2. Mathematical expressions of multimodal benchmark functions.

| Function Expressions |
|--|
| $F17 = \sum_{i=1}^n [x_i^2 - 10 \cos(2\pi x_i) + 10]$ |
| $F18 = 1 + \sum_{i=1}^n \sin^2(x_i) - 0.1e^{(\sum_{i=1}^n x_i^2)}$ |
| $F19 = \sum_{i=1}^n x_i \sin(x_i) + 0.1x_i $ |
| $F20 = \sum_{i=1}^n \epsilon_i x_i ^i$ |
| $F21 = -20 \exp\left(-0.2\sqrt{\frac{1}{n} \times \sum_{i=1}^n x_i^2}\right) - \exp\left(\frac{1}{n} \times \sum_{i=1}^n \cos(2\pi x_i)\right) + 20 + e$ |
| $F22 = \sum_{i=1}^n 8 \sin^2[7(x_i - 0.9)^2] + 6 \sin^2[14(x_1 - 0.9)^2] + (x_i - 0.9)^2$ |
| $F23 = 1 - \cos\left(2\pi\sqrt{\sum_{i=1}^n x_i^2}\right) + 0.1\sqrt{\sum_{i=1}^n x_i^2}$ |
| $F24 = \frac{1}{4000} \sum_{i=1}^n x_i^2 - \prod_{i=1}^n \cos\left(\frac{x_i}{\sqrt{i}}\right) + 1$ |
| $F25 = 0.1 \left\{ \sin^2(3\pi x_1) + \sum_{i=1}^n (x_i - 1)^2 [1 + \sin^2(3\pi x_i + 1)] + (x_n - 1)^2 [1 + \sin^2(2\pi x_n)] \right\} + \sum_{i=1}^n u(x_i, 5, 100, 4)$ |
| $F26 = \frac{\pi}{n} \left\{ 10 \sin(\pi y_i) + \sum_{i=1}^{n-1} (y_i - 1)^2 [1 + 10 \sin^2(\pi y_{i+1})] + (y_n - 1)^2 \right\} + \sum_{i=1}^n u(x_i, 10, 100, 4)$ |
| $F27 = x^2 + y^2 + 25[\sin^2(x) + \sin^2(y)]$ |
| $F28 = \sin(x)e^{(1-\cos(y))^2} + \cos(y)e^{(1-\sin(x))^2} + (x - y)^2$ |
| $F29 = \left[1 + (x_1 + x_2 + 1)^2 (19 - 14x_1 + 3x_1^2 - 14x_2 + 6x_1x_2 + 3x_2^2) \right] \times \left[30 + (2x_1 - 3x_2)^2 (18 - 32x_1 + 12x_1^2 + 48x_2 - 36x_1x_2 + 27x_2^2) \right]$ |
| $F30 = x^2 + y^2 + xy + \sin(x) + \cos(y) $ |

Table A3. Mathematical expressions of fixed-dimension functions.

| Function Expressions |
|---|
| $F31 = \left(\frac{1}{500} + \sum_{j=1}^{25} \frac{1}{j + \sum_{i=1}^2 (x_i - a_{ij})^6} \right)^{-1}$ |
| $F32 = \sum_{i=1}^{11} \left[a_i - \frac{x_1 (b_i^2 + b_i x_2)}{b_i^2 + b_i x_3 + x_4} \right]^2$ |
| $F33 = - \sum_{i=1}^4 c_i \exp \left[- \sum_{j=1}^4 a_{ij} (x_j - p_{ij}) \right]$ |
| $F34 = - \sum_{i=1}^5 \left[(x - a_i)(x - a_i)^T + c_i \right]^{-1}$ |
| $F35 = - \sum_{i=1}^7 \left[(x - a_i)(x - a_i)^T + c_i \right]^{-1}$ |
| $F36 = - \sum_{i=1}^{10} \left[(x - a_i)(x - a_i)^T + c_i \right]^{-1}$ |

References

1. Qu, B.Y.; Liang, J.J.; Suganthan, P.N. Niching particle swarm optimization with local search for multi-modal optimization. *Inf. Sci.* **2012**, *197*, 131–143. [\[CrossRef\]](#)
2. Mohapatra, P.; Das, K.N.; Roy, S. A modified competitive swarm optimizer for large scale optimization problems. *Appl. Soft Comput.* **2017**, *59*, 340–362. [\[CrossRef\]](#)
3. Wang, L.Y.; Zhao, W.G.; Tian, Y.L.; Pan, G.Z. A bare bones bacterial foraging optimization algorithm. *Cogn. Syst. Res.* **2018**, *52*, 301–311. [\[CrossRef\]](#)
4. Holland, J.H. Genetic algorithms. *Sci. Am.* **1992**, *267*, 66–72. [\[CrossRef\]](#)
5. Kirkpatrick, S.; Gelatt, C.D., Jr.; Vecchi, M.P. Optimization by simulated annealing. *Science* **1983**, *220*, 671–680. [\[CrossRef\]](#)
6. Hatamlou, A. Black hole: A new heuristic optimization approach for data clustering. *Inf. Sci.* **2013**, *222*, 175–184. [\[CrossRef\]](#)
7. Formato, R.A. Central force optimization: A new metaheuristic with applications in applied electromagnetics. *Prog. Electromagn. Res.* **2007**, *77*, 425–491. [\[CrossRef\]](#)
8. Eskandar, H.; Sadollah, A.; Bahreininejad, A.; Hamdi, M. Water cycle algorithm—A novel metaheuristic optimization method for solving constrained engineering optimization problems. *Comput. Struct.* **2012**, *110*, 151–166. [\[CrossRef\]](#)
9. Nematollahi, A.F.; Rahiminejad, A.; Vahidi, B. A novel physical based meta-heuristic optimization method known as Lightning Attachment Procedure Optimization. *Appl. Soft Comput.* **2017**, *59*, 596–621. [\[CrossRef\]](#)
10. Rao, R.V.; Savsani, V.J.; Vakharia, D.P. Teaching-learning-based optimization: A novel method for constrained mechanical design optimization problems. *Comput. Aided Design* **2011**, *43*, 303–315. [\[CrossRef\]](#)
11. Askari, Q.; Younas, I.; Saeed, M. Political Optimizer: A novel socio-inspired meta-heuristic for global optimization. *Knowl.-Based Syst.* **2020**, *195*, 105709. [\[CrossRef\]](#)
12. Dong, J.; Zou, H.; Li, W.; Wang, M. A hybrid greedy political optimizer with fireworks algorithm for numerical and engineering optimization problems. *Sci. Rep.* **2022**, *12*, 13243. [\[CrossRef\]](#)
13. Kennedy, J.; Eberhart, R. Particle swarm optimization. In Proceedings of the ICNN'95—International Conference on Neural Networks, Perth, WA, Australia, 27 November–1 December 1995; Volume 1944, pp. 1942–1948.
14. Dong, J.; Li, Q.; Deng, L. Design of fragment-type antenna structure using an improved BPSO. *IEEE Trans. Antennas Propag.* **2017**, *66*, 564–571. [\[CrossRef\]](#)
15. Dorigo, M.; Birattari, M.; Stutzle, T. Ant colony optimization. *IEEE Comput. Intell. Mag.* **2006**, *1*, 28–39. [\[CrossRef\]](#)
16. Basturk, B.; Karaboga, D. An artificial bee colony (ABC) algorithm for numeric function optimization. In Proceedings of the IEEE Swarm Intelligence Symposium, Indianapolis, IN, USA, 12–14 May 2006.
17. Krishnanand, K.N.; Ghose, D. Glowworm Swarm Optimisation: A New Method for Optimising Multi-Modal Functions. *Int. J. Comput. Intell. Stud.* **2009**, *1*, 93. [\[CrossRef\]](#)
18. Askarzadeh, A. A novel metaheuristic method for solving constrained engineering optimization problems: Crow search algorithm. *Comput. Struct.* **2016**, *169*, 1–12. [\[CrossRef\]](#)
19. Shadravan, S.; Naji, H.R.; Bardsiri, V.K. The Sailfish Optimizer: A novel nature-inspired metaheuristic algorithm for solving constrained engineering optimization problems. *Eng. Appl. Artif. Intell.* **2019**, *80*, 20–34. [\[CrossRef\]](#)
20. Heidari, A.A.; Mirjalili, S.; Faris, H.; Aljarah, I.; Mafarja, M.; Chen, H.L. Harris hawks optimization: Algorithm and applications. *Future Gener. Comput. Syst.* **2019**, *97*, 849–872. [\[CrossRef\]](#)
21. Li, W.; Shi, R.; Dong, J. Harris hawks optimizer based on the novice protection tournament for numerical and engineering optimization problems. *Appl. Intell.* **2022**, 1–26. [\[CrossRef\]](#)
22. Zhao, W.G.; Zhang, Z.X.; Wang, L.Y. Manta ray foraging optimization: An effective bio-inspired optimizer for engineering applications. *Eng. Appl. Artif. Intell.* **2020**, *87*, 103300. [\[CrossRef\]](#)

23. Zervoudakis, K.; Tsafarakis, S. A mayfly optimization algorithm. *Comput. Ind. Eng.* **2020**, *145*, 106559. [[CrossRef](#)]
24. Mirjalili, S.; Lewis, A. The Whale Optimization Algorithm. *Adv. Eng. Softw.* **2016**, *95*, 51–67. [[CrossRef](#)]
25. Alsattar, H.A.; Zaidan, A.A.; Zaidan, B.B. Novel meta-heuristic bald eagle search optimisation algorithm. *Artif. Intell. Rev.* **2020**, *53*, 2237–2264. [[CrossRef](#)]
26. Pecora, L.M.; Carroll, T.L. Synchronization in chaotic systems. *Phys. Rev. Lett.* **1990**, *64*, 821–824. [[CrossRef](#)]
27. Feng, J.H.; Zhang, J.; Zhu, X.S.; Lian, W.W. A novel chaos optimization algorithm. *Multimed. Tools Appl.* **2017**, *76*, 17405–17436. [[CrossRef](#)]
28. Ouertani, M.W.; Manita, G.; Korbaa, O. Chaotic lightning search algorithm. *Soft Comput.* **2021**, *25*, 2039–2055. [[CrossRef](#)]
29. Alatas, B. Chaotic bee colony algorithms for global numerical optimization. *Expert Syst. Appl.* **2010**, *37*, 5682–5687. [[CrossRef](#)]
30. Kohli, M.; Arora, S. Chaotic grey wolf optimization algorithm for constrained optimization problems. *J. Comput. Des. Eng.* **2018**, *5*, 458–472. [[CrossRef](#)]
31. Arora, S.; Singh, S. An improved butterfly optimization algorithm with chaos. *J. Intell. Fuzzy Syst.* **2017**, *32*, 1079–1088. [[CrossRef](#)]
32. Gandomi, A.H.; Yang, X.S.; Talatahari, S.; Alavi, A.H. Firefly algorithm with chaos. *Commun. Nonlinear Sci.* **2013**, *18*, 89–98. [[CrossRef](#)]
33. Reynolds, A.M.; Frye, M.A. Free-Flight Odor Tracking in *Drosophila* Is Consistent with an Optimal Intermittent Scale-Free Search. *PLoS ONE* **2007**, *2*, e354. [[CrossRef](#)] [[PubMed](#)]
34. Viswanathan, G.M.; Afanasyev, V.; Buldyrev, S.V.; Murphy, E.J.; Prince, P.A.; Stanley, H.E. Lévy flight search patterns of wandering albatrosses. *Nature* **1996**, *381*, 413–415. [[CrossRef](#)]
35. Viswanathan, G.M. Fish in Lévy-flight foraging. *Nature* **2010**, *465*, 1018–1019. [[CrossRef](#)] [[PubMed](#)]
36. Gandomi, A.H.; Yang, X.-S.; Alavi, A.H. Cuckoo search algorithm: A metaheuristic approach to solve structural optimization problems. *Eng. Comput.* **2013**, *29*, 17–35. [[CrossRef](#)]
37. Emary, E.; Zawbaa, H.M.; Sharawi, M. Impact of Lévy flight on modern meta-heuristic optimizers. *Appl. Soft Comput.* **2019**, *75*, 775–789. [[CrossRef](#)]
38. Yang, X.-S. Flower pollination algorithm for global optimization. In Proceedings of the International Conference on Unconventional Computing and Natural Computation, Orléans, France, 3–7 September 2012; pp. 240–249.
39. Amirsadri, S.; Mousavirad, S.J.; Ebrahimpour-Komleh, H. A Levy flight-based grey wolf optimizer combined with back-propagation algorithm for neural network training. *Neural Comput. Appl.* **2018**, *30*, 3707–3720. [[CrossRef](#)]
40. Tubishat, M.; Ja'afar, S.; Idris, N.; Al-Betar, M.A.; Alswaitti, M.; Jarrah, H.; Ismail, M.A.; Omar, M.S. Improved sine cosine algorithm with simulated annealing and singer chaotic map for Hadith classification. *Neural Comput. Appl.* **2022**, *34*, 1385–1406. [[CrossRef](#)]
41. Talatahari, S.; Kaveh, A.; Sheikholeslami, R. Chaotic imperialist competitive algorithm for optimum design of truss structures. *Struct. Multidiscip. Optim.* **2012**, *46*, 355–367. [[CrossRef](#)]
42. Wang, G.-G.; Guo, L.; Gandomi, A.H.; Hao, G.-S.; Wang, H. Chaotic Krill Herd algorithm. *Inf. Sci.* **2014**, *274*, 17–34. [[CrossRef](#)]
43. Houssein, E.H.; Helmy, B.E.D.; Elngar, A.A.; Abdelminaam, D.S.; Shaban, H. An Improved Tunicate Swarm Algorithm for Global Optimization and Image Segmentation. *IEEE Access* **2021**, *9*, 56066–56092. [[CrossRef](#)]
44. Gharehchopogh, F.S. An Improved Tunicate Swarm Algorithm with Best-random Mutation Strategy for Global Optimization Problems. *J. Bionic Eng.* **2022**, *19*, 1177–1202. [[CrossRef](#)]
45. Kaur, S.; Awasthi, L.K.; Sangal, A.L.; Dhiman, G. Tunicate Swarm Algorithm: A new bio-inspired based metaheuristic paradigm for global optimization. *Eng. Appl. Artif. Intell.* **2020**, *90*, 103541. [[CrossRef](#)]
46. Chawla, M.; Duhan, M. Levy Flights in Metaheuristics Optimization Algorithms—A Review. *Appl. Artif. Intell.* **2018**, *32*, 802–821. [[CrossRef](#)]
47. Chegini, S.N.; Bagheri, A.; Najafi, F. PSOSCALF: A new hybrid PSO based on Sine Cosine Algorithm and Levy flight for solving optimization problems. *Appl. Soft Comput.* **2018**, *73*, 697–726. [[CrossRef](#)]
48. Hakli, H.; Uguz, H. A novel particle swarm optimization algorithm with Levy flight. *Appl. Soft Comput.* **2014**, *23*, 333–345. [[CrossRef](#)]
49. Yan, B.L.; Zhao, Z.; Zhou, Y.C.; Yuan, W.Y.; Li, J.; Wu, J.; Cheng, D.J. A particle swarm optimization algorithm with random learning mechanism and Levy flight for optimization of atomic clusters. *Comput. Phys. Commun.* **2017**, *219*, 79–86. [[CrossRef](#)]
50. Emary, E.; Zawbaa, H.M. Impact of Chaos Functions on Modern Swarm Optimizers. *PLoS ONE* **2016**, *11*, e158738. [[CrossRef](#)]
51. Caponetto, R.; Fortuna, L.; Fazzino, S.; Xibilia, M.G. Chaotic sequences to improve the performance of evolutionary algorithms. *IEEE Trans. Evolut. Comput.* **2003**, *7*, 289–304. [[CrossRef](#)]
52. Jordehi, A.R. Chaotic bat swarm optimisation (CBSO). *Appl. Soft Comput.* **2015**, *26*, 523–530. [[CrossRef](#)]
53. Zheng, W.-M. Kneading plane of the circle map. *Chaos Solitons Fractals* **1994**, *4*, 1221–1233. [[CrossRef](#)]
54. Bucolo, M.; Caponetto, R.; Fortuna, L.; Frasca, M.; Rizzo, A. Does chaos work better than noise? *IEEE Circuits Syst. Mag.* **2002**, *2*, 4–19. [[CrossRef](#)]
55. He, D.; He, C.; Jiang, L.G.; Zhu, H.W.; Hu, G.R. Chaotic characteristics of a one-dimensional iterative map with infinite collapses. *IEEE Trans. Circuits Syst. I* **2001**, *48*, 900–906. [[CrossRef](#)]
56. May, R.M. Simple mathematical models with very complicated dynamics. *Nature* **1976**, *261*, 459–467. [[CrossRef](#)]
57. Peitgen, H.O.; Jürgens, H.; Saupe, D. *Chaos and Fractals: New Frontiers of Science*; Springer: Berlin/Heidelberg, Germany, 2004.

58. Tavazoei, M.S.; Haeri, M. Comparison of different one-dimensional maps as chaotic search pattern in chaos optimization algorithms. *Appl. Math. Comput.* **2007**, *187*, 1076–1085. [[CrossRef](#)]
59. Igiri, C.P.; Singh, Y.; Bhargava, D. An improved African Buffalo Optimization Algorithm Using Chaotic Map and Chaotic-Levy Flight. *Int. J. Eng. Technol.* **2018**, *7*, 4570–4576.
60. Lin, J.H.; Chou, C.W.; Yang, C.H.; Tsai, H.L. A Chaotic Levy Flight Bat Algorithm for Parameter Estimation in Nonlinear Dynamic Biological Systems. *Comput. Inf. Technol.* **2012**, *2*, 56–63.
61. Mirjalili, S.; Mirjalili, S.M.; Lewis, A. Grey Wolf Optimizer. *Adv. Eng. Softw.* **2014**, *69*, 46–61. [[CrossRef](#)]
62. Mirjalili, S. SCA: A Sine Cosine Algorithm for solving optimization problems. *Knowl.-Based Syst.* **2016**, *96*, 120–133. [[CrossRef](#)]
63. Xue, J.K.; Shen, B. A novel swarm intelligence optimization approach: Sparrow search algorithm. *Syst. Sci. Control Eng.* **2020**, *8*, 22–34. [[CrossRef](#)]
64. Faramarzi, A.; Heidarinejad, M.; Mirjalili, S.; Gandomi, A.H. Marine Predators Algorithm: A nature-inspired metaheuristic. *Expert Syst. Appl.* **2020**, *152*, 113377. [[CrossRef](#)]
65. Zhou, Y.Q.; Zhou, G.; Zhang, J.L. A hybrid glowworm swarm optimization algorithm to solve constrained multimodal functions optimization. *Optimization* **2015**, *64*, 1057–1080. [[CrossRef](#)]
66. Shukla, A. Chaos teaching learning based algorithm for large-scale global optimization problem and its application. *Concurr. Comput. Pract. Exp.* **2021**, *34*, e6514. [[CrossRef](#)]
67. Mirjalili, S.; Mirjalili, S.M.; Hatamlou, A. Multi-Verse Optimizer: A nature-inspired algorithm for global optimization. *Neural Comput. Appl.* **2016**, *27*, 495–513. [[CrossRef](#)]
68. Coello, C.A.C. Use of a self-adaptive penalty approach for engineering optimization problems. *Comput. Ind.* **2000**, *41*, 113–127. [[CrossRef](#)]
69. Kumar, A.; Wu, G.H.; Ali, M.Z.; Mallipeddi, R.; Suganthan, P.N.; Das, S. A test-suite of non-convex constrained optimization problems from the real-world and some baseline results. *Swarm. Evol. Comput.* **2020**, *56*, 100693. [[CrossRef](#)]